Title

Effect of Light Biocementation on the Liquefaction Triggering and Post-Triggering Behavior of Loose Sands

Journal

Journal of Geotechnical and Geoenvironmental Engineering, 148(1)

ISSN

1090-0241

Authors

Lee, Minyong
Gomez, Michael G
Kortbawi, Maya El
et al.

Publication Date

2022

DOI

10.1061/(asce)gt.1943-5606.0002707

Peer reviewed

Effect of Light Biocementation on the Liquefaction Triggering and Post-Triggering Behavior of Loose Sands

Minyong Lee, S.M.ASCE[1]; Michael G. Gomez, M.ASCE[2]; Maya El Kortbawi, S.M.ASCE[3]; and Katerina Ziotopoulou, M.ASCE[4]

Abstract: Microbially induced calcite precipitation (MICP) is an environmentally conscious ground-improvement method that can enhance the engineering properties of granular soils through the precipitation of calcium carbonate ($CaCO_3$) on soil particle surfaces and contacts. Although numerous studies have shown the ability of biocementation to improve the liquefaction resistance of loose sands, the effects of light cementation levels on undrained cyclic behaviors have remained relatively unexplored. A series of undrained monotonic and cyclic direct simple shear tests were performed to examine the effect of light biocementation ($\Delta V_s < 100$ m/s and $CaCO_3$ contents <0.9%) on the liquefaction triggering and post-triggering behavior of loose Ottawa F-65 sand subjected to varying loading magnitudes [cyclic stress ratio (CSR) = 0.1 to 0.3]. Results suggest that the presence of light biocementation can significantly improve the liquefaction triggering resistance of loose sands, with log-linear increases in the number of cycles required to trigger liquefaction, which consistently correlated with cementation-induced V_s increases. Despite these remarkable pretriggering improvements, almost no improvements were observed in post-triggering strain accumulation and postcyclic reconsolidation behaviors, with V_s measurements indicating that small-strain improvements were largely erased following shearing events. **DOI: 10.1061/(ASCE)GT.1943-5606.0002707.**

Author keywords: Biogeotechnics; Biocementation; MICP; Liquefaction; Calcite; Cemented sands; Ground improvement.

Introduction

Traditional geotechnical ground-improvement methods use high mechanical energy and energy-intensive materials to improve soil engineering properties, consequently resulting in considerable greenhouse gas emissions, potential for groundwater contamination, and other impacts on environmental quality (Karol 2003; DeJong et al. 2010; Kendall et al. 2018). Sparked, in part, by increased awareness of the environmental consequences of conventional geotechnical soil improvement methods, biomediated soil-improvement technologies have been recently developed to achieve engineering performances comparable to conventional techniques (e.g., chemical grouting and deep dynamic compaction) while achieving significant environmental benefits (Seagren and Aydilek 2010; DeJong et al. 2010, 2013). Microbially induced calcite precipitation (MICP) is one such technology that can improve the engineering properties of granular soils through the precipitation of calcium carbonate ($CaCO_3$) minerals on soil particle surfaces and contacts (Ferris et al. 1996; Stocks-Fischer et al. 1999; DeJong et al. 2006).

In the biocementation process, microorganisms containing urease enzymes catalyze a hydrolysis reaction that degrades supplied urea, producing carbonate ions and alkalinity (Mobley et al. 1995; Stocks-Fischer et al. 1999). When sufficient calcium ions are supplied via treatment solutions or surrounding groundwater, the production of carbonate ions from ureolysis may enable supersaturation of soil pore fluids with respect to calcium carbonate ($CaCO_3$) minerals, thereby enabling precipitation (Ferris et al. 2004; Gomez et al. 2019). The resulting biocementation can dramatically increase the shear strength and stiffness of soils (DeJong et al. 2006; Montoya and DeJong 2015; Gomez et al. 2018a; Nafisi et al. 2020) with generally only minor reductions in hydraulic conductivities for clean sandy soils (Gomez and DeJong 2017; San Pablo et al. 2020).

Biocementation has been proposed for a wide range of engineering applications including geotechnical soil improvement (Martinez and DeJong 2009; van Paassen et al. 2010; Feng and Montoya 2016; Gomez et al. 2017; Lin et al. 2016; Gao et al. 2019; Xiao et al. 2020; and many others), rock fracture sealing (Cuthbert et al. 2013; Phillips et al. 2016; Minto et al. 2016), soil scour and erosion prevention (Gomez et al. 2015; Montoya et al. 2018; Tao et al. 2018; Ghasemi and Montoya 2020), divalent contaminant immobilization (Fujita et al. 2004; Bhattacharya et al. 2018; He et al. 2019; Jiang et al. 2019), concrete repair (Ramakrishnan et al. 1998, 2001; Ramachandran et al. 2001; De Muynck et al. 2008), and construction material development (Bernardi et al. 2014; Choi et al. 2016; Li et al. 2016, 2020; Xiao et al. 2019b).

Of these potential applications, MICP has been most notably proposed as an environmentally conscious method to mitigate earthquake-induced soil liquefaction (Montoya et al. 2013; Darby et al. 2019; Lee et al. 2020; and others). Biocementation improves soil undrained cyclic behaviors through a variety of different mechanisms including (1) $CaCO_3$ bonding between soil particles, which limits soil particle movements and contractive tendencies during cyclic shearing, (2) increases in soil dry densities resulting from precipitated $CaCO_3$ mineral solids that densify soils and increase

[1]Ph.D. Student, Dept. of Civil and Environmental Engineering, Univ. of Washington, Seattle, WA 98195. ORCID: https://orcid.org/0000-0002-7436-5374. Email: my0321@uw.edu

[2]Assistant Professor, Dept. of Civil and Environmental Engineering, Univ. of Washington, Seattle, WA 98105 (corresponding author). ORCID: https://orcid.org/0000-0002-4464-5447. Email: mggomez@uw.edu

[3]Ph.D. Student, Dept. of Civil and Environmental Engineering, Univ. of California, Davis, CA 95616. ORCID: https://orcid.org/0000-0002-5675-1554. Email: melkortbawi@ucdavis.edu

[4]Assistant Professor, Dept. of Civil and Environmental Engineering, Univ. of California, Davis, CA 95616. ORCID: https://orcid.org/0000-0001-5494-497X. Email: kziotopoulou@ucdavis.edu

Note. This manuscript was submitted on October 21, 2020; approved on August 20, 2021; published online on October 21, 2021. Discussion period open until March 21, 2022; separate discussions must be submitted for individual papers. This paper is part of the ***Journal of Geotechnical and Geoenvironmental Engineering***, © ASCE, ISSN 1090-0241.

dilative tendencies at larger strains, and (3) $CaCO_3$ soil particle coatings that can increase soil particle surface roughnesses and interparticle frictional resistances. Collectively, these mechanisms suggest that at small strains, when the integrity of cemented bonds is maintained, and at larger strains, when cemented bonds are sheared and destructured, the presence of biocementation can improve soil shearing behaviors. Although such mechanisms have been extensively described by prior researchers (DeJong et al. 2010; and others), the magnitudes of biocementation needed to mobilize each of these mechanisms and their respective individual and combined effects on soil behaviors during undrained cyclic loading have remained less clear.

Metrics to characterize each of the aforementioned individual mechanisms have not been agreed upon in past literature; however, it is hypothesized that (1) $CaCO_3$ bonding between soil particles may be best assessed using small-strain stiffness measurements (e.g., shear-wave velocity changes); (2) improvements in large-strain behaviors resulting from precipitated $CaCO_3$ solids may be best described using soil dry density, $CaCO_3$ content measurements, and mechanical testing; and (3) increases in soil particle surface roughnesses may be characterized using direct imaging of soil specimens and large-strain mechanical testing.

Numerous studies have examined the effect of $CaCO_3$ biocementation on the undrained cyclic behavior of sands. Studies have overwhelmingly concluded that the addition of biocementation increases soil cyclic resistances, with magnitudes of improvement generally correlating to cementation levels quantified by $CaCO_3$ contents and/or shear-wave velocity (V_s) increases (Montoya et al. 2013 and others). More recent studies have significantly furthered our understanding of how biocemented materials may behave under a range of different conditions including various cementation levels, applied loadings, confining stresses, and fines contents. For example, Simatupang et al. (2018) performed undrained cyclic triaxial tests on lightly biocemented Toyoura and Keisha No. 4 sand specimens improved using enzymatically induced carbonate precipitation (EICP) with $CaCO_3$ contents of less than 0.8%. Although pretriggering behaviors appeared to be primarily governed by interparticle $CaCO_3$ bonding, as described by shear-wave velocity increases (ΔV_s), improvements in post-triggering strain accumulation behaviors appeared to primarily reflect $CaCO_3$-induced increases in soil dry densities.

Zamani and Montoya (2019) performed undrained cyclic direct simple shear (DSS) tests on biocemented silty sand specimens and found that when ΔV_s increases were near 300 m/s, significant improvements in liquefaction triggering were achieved, with observed improvements also significantly influenced by soil fines contents. Xiao et al. (2019a) conducted a series of undrained cyclic triaxial tests on biocemented calcareous sands prepared to different initial relative densities (D_r) and concluded that the effect of biocementation on liquefaction triggering was more beneficial than that which could be attributed to cementation-induced dry-density changes alone, with large benefits afforded by the presence of cohesive bonds.

Darby et al. (2019) performed a series of centrifuge tests on untreated and biocemented loose ($D_r \approx 38\%$) Ottawa F-65 sand specimens subjected to multiple shaking events and found that when ΔV_s increases were near and above 60 m/s, significant increases in peak base accelerations were required to trigger liquefaction. Following the initial triggering event, these biocemented specimens also maintained greater resistances to triggering during subsequent loading events when compared with similar uncemented specimens, suggesting that cementation-induced improvements persisted following triggering. Riveros and Sadrekarimi (2020) performed undrained cyclic DSS tests on biocemented Fraser River sand specimens with ΔV_s increases near 90 m/s and observed significant changes in pretriggering excess pore-pressure generation, which transitioned from rapid increases in uncemented specimens to more gradual and steady development with cycles in biocemented materials.

Although prior studies have provided significant insights regarding the potential of biocementation for liquefaction mitigation applications, to date, the spectrum of pretriggering and post-triggering behaviors of sands near the transition from uncemented to lightly cemented conditions has remained poorly characterized. An improved understanding of the effect of low levels of biocementation may not only improve our understanding of MICP soil improvement, but may also provide a unique opportunity to better understand the behavior of naturally cemented soils, many of which involve weak bonding between particles resulting from cold-welding and light mineral coatings (Mitchell 2008). The importance of even small amounts of cementation on the behavior of natural geomaterials has long been recognized (Saxena and Lastrico 1978; Clough et al. 1981, 1989; Rad and Clough 1982; Saxena et al. 1988), however, a systematic study of its effects has remained challenging due to sample disturbance limitations (Frydman et al. 1980; Bachus et al. 1981; Clough and Bachus 1981; and others) and the limited sensitivity of traditional large-strain in situ testing instruments to light cementation levels (Rad and Tumay 1986; Akili and Nabil 1988; Puppala et al. 1993; and others). Even when high-quality naturally cemented sand samples can be identified, researchers are unable to control specimen initial conditions (e.g., cementation magnitudes, initial D_r, curing stresses, and others), and cementation heterogeneity and disturbances resulting from stress relief are unavoidable.

Acknowledging these limitations, researchers have turned toward artificial cementation agents, such as portland cement, to recreate natural cementation in the laboratory. Although potentially representative of some ground-improvement processes, many of these cementation agents exhibit increased ductility when compared with naturally cemented geomaterials. Biocementation may afford significant advantages with respect to these aspects through the transformative ability to recreate perfectly cemented soil specimens in the laboratory using $CaCO_3$ mineral bonds that are likely more mineralogically and mechanically representative of natural cementation (Ismail et al. 2002; DeJong et al. 2006; Gomez et al. 2018a).

In this study, a DSS testing program was performed to further our understanding of the effect of light levels of biocementation on the undrained monotonic and cyclic behavior of loose poorly graded sands. Although various definitions have been proposed to describe light, moderate, and heavy biocementation levels (Montoya and DeJong 2015; Nafisi et al. 2020; and others), in this study, we refer to the achieved specimens that had cementation-induced ΔV_s increases of 100 m/s or less as being lightly cemented. Twenty-eight undrained cyclic DSS tests were performed on biocemented Ottawa F-65 sand specimens prepared to loose initial relative densities ($D_r \approx 30\%$) and treated to varying cementation levels corresponding to ΔV_s increases ranging from 0 to 100 m/s and $CaCO_3$ contents from 0% to 0.9% with applied cyclic stress ratios (CSRs) ranging from 0.1 to 0.3 ($\sigma'_{v\,\text{initial}} = 100$ kPa).

In addition, 34 undrained cyclic DSS tests were performed on uncemented specimens prepared to loose ($D_r \approx 30\%$), medium-dense ($D_r \approx 55\%$), and dense ($D_r \approx 75\%$) initial relative densities with identical applied CSRs in order to compare the behavior of biocemented specimens with that of similar uncemented specimens and to benchmark improvements resulting from biocementation through comparisons with improvements achievable via soil densification. In all cyclic tests, the shearing phase was followed by drained reconsolidation to the initial overburden stress. Following the cyclic testing program, seven undrained monotonic tests were performed on loose biocemented specimens treated to similarly light biocementation levels ($\Delta V_s = 0$ to 93 m/s) to further explore the effect of light cementation on soil stress–strain behaviors and

compare monotonic behaviors with previous results from cyclic testing. For all specimens, V_s and D_r values were characterized prior to shearing events.

For biocemented specimens, changes in D_r, $CaCO_3$ contents, and V_s values resulting from the biocementation process were also assessed. Following testing, relationships between specimen properties, including D_r and biocementation magnitudes, and observed behaviors, including pretriggering excess pore-pressure generation, post-triggering strain accumulation, and postshearing reconsolidation strains, and V_s changes were examined. The achieved results provide new understandings regarding the effect of light levels of biocementation on soil pretriggering and post-triggering behaviors and offer new insights regarding how biocementation degrades during undrained cyclic loading and how its influence on soil behavior evolves during the shearing process.

Materials and Methods

Sand Material

All tests involved Ottawa F-65 sand (US Silica, Ottawa, Illinois) following previous investigations by Ziotopoulou et al. (2018), Darby et al. (2019), Carey et al. (2020), Burdalski and Gomez (2020), El Ghoraiby et al. (2020), and others. The sand had a D_{10} of 0.13 mm, D_{30} of 0.18 mm, D_{50} of 0.21 mm, D_{60} of 0.23 mm, no fines (Carey et al. 2020), and a USCS classification of SP following ASTM D2487-17e1 (ASTM 2017). The minimum and maximum void ratios for this sand were 0.51 and 0.78, respectively, following ASTM D4253-16e1 and ASTM D4254-16 (ASTM 2016a, b) as reported by Carey et al. (2020). Although the effect of soil type was not considered in this study, Ottawa F-65 sand was selected for lab testing due to its chemically inert quartz mineralogy, near-uniform grain-size distribution, and low fines content. These attributes were expected to be advantageous for this particular study because they allowed for other potentially complicating factors related to changes in specimen fines contents, gradations, and other variables to be minimized and therefore the effect of light levels of biocementation on soil behaviors to be better isolated.

Direct Simple Shear Apparatus

Fig. 1 provides images of the direct simple shear testing apparatus, shear- and pressure-wave monitoring system, treatment solution application system, and specimen configuration. An electromechanical dynamic cyclic simple shear apparatus (EMDCSS) (GDS Instruments, Hook, UK) was used to perform all monotonic and cyclic tests. The apparatus included several load cells and LVDTs to measure applied axial forces (5-kN range and 0.045% accuracy), shear forces (5-kN range and 0.045% accuracy), axial displacements (25-mm range and 0.1% accuracy), and shear displacements (15-mm range and 0.1% accuracy). All tests involved pinned porous stone disks (2-mm pin lengths) to limit potential shear localization at soil–top platen interfaces. A ring retainment system was used to limit potential rocking of DSS rings during shearing.

Specimen Preparation

DSS specimens were dry-pluviated using a custom-fabricated pluviation device, and the pluviator aperture was adjusted while maintaining a constant fall height to achieve different targeted relative densities. Specimens were 70.22 mm in diameter and had heights near 22 mm. After pluviation, samples were placed within the DSS loading frame, and a vertical effective stress of 100 kPa was applied to simulate stress conditions near 10 m within a saturated soil deposit. Following stress application, a series of small-amplitude strain-controlled drained cycles were applied to all specimens to ensure proper engagement of specimens at the porous disk and soil interface, as well as to establish K_0 conditions throughout specimens.

A series of preconditioning protocol development tests were performed prior to this study to determine the appropriate number of drained cycles needed to properly engage specimens without resulting in densification. A protocol was selected wherein 75

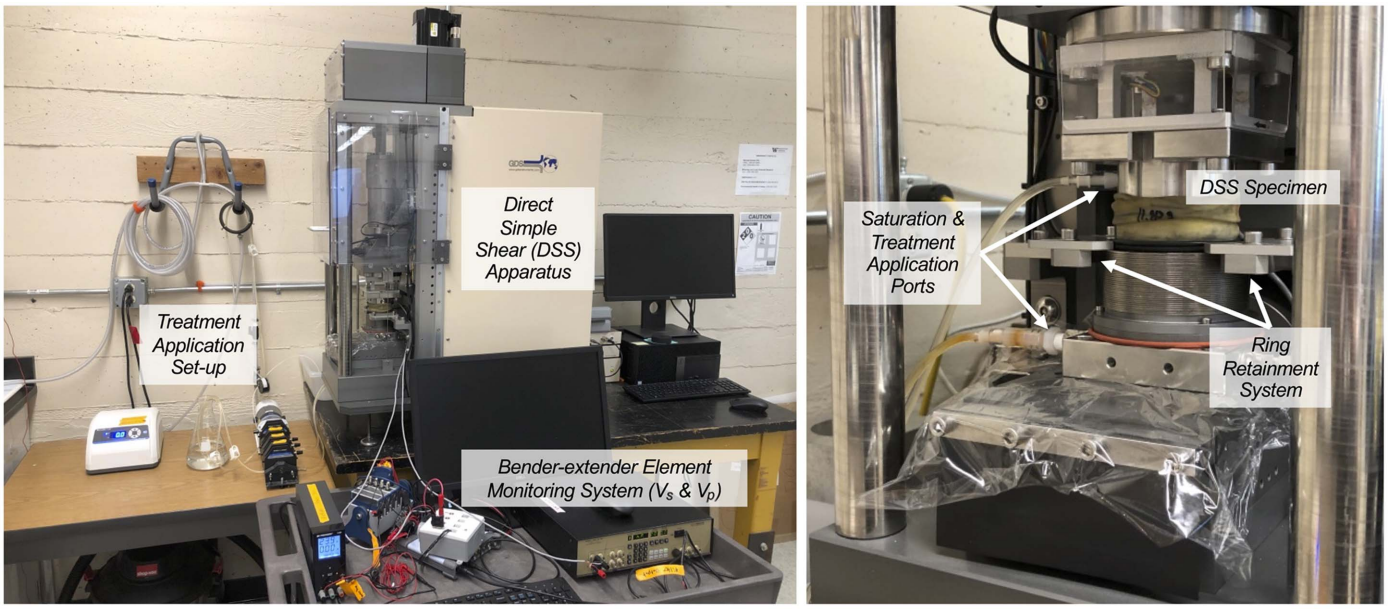

Fig. 1. (a) DSS testing apparatus, treatment application setup, and bender-extender element monitoring system; and (b) DSS specimen configuration including saturation and treatment application ports and ring retainment system.

J. Geotech. Geoenviron. Eng., 2022, 148(1): 04021170

small-strain, strain-controlled drained cycles (amplitude of 0.01 mm and 0.05% shear strain) were performed immediately following pluviation and before saturation and biocementation treatments. This protocol was identified by (1) analyzing changes in specimen relative densities and stiffnesses resulting from the application of varying numbers of small-strain drained cycles, and (2) comparing the number of loading cycles required to trigger liquefaction for preconditioned specimens with past independent experimental data available for Ottawa F-65 sand (Ueda et al. 2018; Morales et al. 2020) to ensure consistency. In all cases, specimen D_r values changed by less than 2% following both initial saturation and small-strain drained cycling.

Following this preconditioning sequence, specimens were saturated with 450 mL (≈12–13 pore volumes) of deionized water that was boiled and deaired using a Nold deaerator device (Geokon, Lebanon, New Hampshire) to eliminate the potential for partial saturation of specimens and matric suction effects. Saturation solutions were pumped slowly from the bottom cap to the top cap for at least 30 min until no bubbles were observed exiting the specimen over a period of 10 min. Saturation was verified using compressional-wave velocity (V_p) measurements from bender-extender elements, and V_p values exceeded 1,400 m/s in specimens before shearing. For untreated specimens, shearing events proceeded immediately after saturation. For biocemented specimens, biocementation treatments were applied following saturation. All reported biocemented specimen total D_r values were calculated for conditions present immediately prior to undrained shearing events at a vertical effective stress of 100 kPa by oven-drying and weighing specimens after testing. Total D_r values therefore account for both dry sand masses as well as additional masses resulting from generated $CaCO_3$ biocementation.

Although the concept of relative density may not hold strictly true for biocemented sands, due to potential soil gradation changes and corresponding changes in e_{min} and e_{max} values, it is unlikely that such effects were significant given the low cementation magnitudes considered herein (<0.9% $CaCO_3$ by mass). The use of total D_r values allowed for the response of biocemented specimens to be compared with other uncemented specimens on the basis of dry density alone. For biocemented specimens, estimates of initial relative densities prior to biocementation ($D_{r\,initial}$), were also further determined from total D_r measurements while removing precipitated $CaCO_3$ masses as informed by measured soil $CaCO_3$ contents. $D_{r\,initial}$ values were identical with total D_r values for uncemented specimens due to the lack of $CaCO_3$ precipitates. The ΔD_r values were also determined and reflect the difference between $D_{r\,initial}$ and total D_r values and therefore reflect the impact of precipitated $CaCO_3$ masses on D_r. All DSS specimens had pore volumes (PVs) between 32 and 35 mL (porosity ≈ 40%).

Biocementation Treatments

Biocemented specimens were augmented prior to cementation using *Sporosarcina pasteurii* (*S. pasteurii*, ATCC 11859) cells at cell densities between 10^7 and 10^8 cells/mL to enable urea hydrolysis and the biocementation process. *S. pasteurii* cells were cultured in sterile ATCC 11,859 growth media (0.13M Tris Base, 20 g/L yeast extract, 10 g/L $(NH_4)_2SO_4$, pH-adjusted to 9.0, autoclaved at 121°C) by inoculating with a frozen stock culture stored at −80°C. Inoculated growth media was incubated for at least 24 h at 30°C using a double-orbital shaker [150 rounds per minute (rpm)]. During the pelleting process, cultured growth media (50 mL) was transferred to a sterile conical tube, centrifuged at 4,150g for 10 min to pellet cells, and the remaining clear supernatant was discarded. Sterile isotonic saline (9 g/L NaCl) was added to rinse pelleted cells, and again the tube was centrifuged and the resulting supernatant was discarded. Sterile saline was then added to obtain a total volume of 10 mL, and the optical density (OD) of this cell suspension was measured at a wavelength of 600 nm (OD_{600}) with a microplate spectrophotometer. Cell densities were estimated from OD_{600} measurements using a lab-specific cell density to OD_{600} calibration curve generated using total direct cell counts (Burdalski 2020). Cell suspensions were added to solutions containing 100 mM urea, and pH and conductivity measurements in time were used to verify ureolytic activity.

Augmentation solution volumes [250 mL (8.3 PV)] were prepared by adding rinsed cell suspensions to deionized water-based solutions containing 100 mM NH_4Cl, 10 mM urea, and 0.2 g/L yeast extract. In order to obtain uniform cell distributions throughout DSS specimens, augmentation solutions were applied in four different injection phases. First, 75 mL (2.5 PV) of augmentation solution was injected from the bottom cap to the top cap at a flow rate of 10 mL/min, and all produced effluent was discarded. Next, 75 mL of the augmentation solution was injected from top to bottom, and all generated effluent was collected and mixed with the remaining 100 mL of fresh augmentation solution. Lastly, 75 mL of this mixture was injected again from bottom to top and then injected again from top to bottom, each time collecting and homogenizing effluent solutions. After injections, augmentation solutions resided within specimens for at least 1 h to encourage cell attachment to soil surfaces prior to cementation injections. During the start of cementation injections, augmentation solution samples were collected to verify that active urea hydrolysis had occurred during augmentation treatments via measured solution pH increases. Although the efficacy of the selected augmentation procedure was not investigated extensively in this study, the procedure was similar to that presented by Gomez et al. (2019), and solution OD_{600} measurements performed before and after augmentation suggested that between 90% and 95% of the injected cells were retained within specimens.

After augmentation, calcium-containing cementation solutions were applied to specimens to initiate biocementation. Cementation solution volumes [250 mL (8.3 PV)] contained 100 mM NH_4Cl and urea and $CaCl_2$ concentrations at a ratio of 1.5 to 1.0. Although urea to calcium concentration ratios were constant, applied $CaCl_2$ concentrations were altered to achieve varying degrees of light cementation as reflected by varying ΔV_s increases. To achieve targeted ΔV_s values between 15 and 100 m/s, $CaCl_2$ concentrations between 50 and 250 mM were applied. Although the authors acknowledge that varying chemical concentrations could have impacted the properties of the achieved $CaCO_3$ precipitation, more extensive investigations by the authors have shown that when applied chemical concentrations are varied between 50 and 500 mM, no significant differences in reaction kinetics, $CaCO_3$ mineralogy, or $CaCO_3$ morphology were observed (Burdalski and Gomez 2020).

During cementation injections, 150 mL (5 PV) cementation solution volumes were injected from the bottom to the top of specimens at a flow rate of 10 mL/min. Cementation solution injections resided within specimens for a minimum of 18 h to ensure reaction completion. For all tests, only a single cementation solution injection was applied. For select tests, fluid samples were collected during saturation injections (which displaced residing cementation solutions), and urea and solution pH measurements were performed and indicated near-full hydrolysis of the injected urea concentrations with post-treatment pH values near 8.4 (Gomez et al. 2018b). After cementation, specimens were resaturated using 450 mL of deaired deionized water that was pH-adjusted to 7.0 using sodium hydroxide to limit potential $CaCO_3$ dissolution. Saturation was again verified using compressional-wave velocity (V_p) measurements from bender-extender elements, and V_p values exceeded

1,400 m/s in specimens before shearing. Measurements of axial strains during treatments suggested that all performed injections had no detectable effects on specimen dry densities.

Several preventative measures were incorporated into the testing program to ensure that specimen porous disks remained pervious following biocementation treatments, including (1) applying only low concentrations of urea (10 mM) during augmentation to limit the potential for abiotic precipitation upon the introduction of calcium during cementation (Gomez et al. 2019); (2) cleaning porous disks with 0.8 M acetic acid and sonication prior to all tests to remove $CaCO_3$ that may have accumulated within disks; and (3) applying cementation solutions at a relatively fast injection rate to limit reactions during solution transport. Observations of injection flow rates during initial saturation, cementation treatment, and post-treatment saturation injections, as well as measured specimen axial strains and applied total stresses, during injections suggested that no detectable clogging of porous stones occurred.

Shear- and Compression-Wave Velocity Measurements

Shear-wave velocity (V_s) measurements were performed for specimens at various points in time using bender-extender elements (Lings and Greening 2001) to verify similar initial conditions between specimens, nondestructively track changes in biocementation magnitudes, and assess postshearing V_s changes related to specimen densification and cementation damage. Bender-extender elements were installed within specimen top and bottom end platens and were excited using a 24-V 100-Hz square wave generated by a signal generator. All received signals were measured and recorded with an oscilloscope using a sampling frequency of 1 MHz. V_s values were determined from known sensor spacings and measurements of shear-wave transmission and arrival times.

V_s measurements were performed for biocemented specimens (1) before and immediately after augmentation, (2) before, immediately after, and ≈18 h after cementation injections, (3) immediately prior to shearing, and (4) after shearing and reconsolidation events. V_s measurements were performed for uncemented specimens (1) immediately before shearing, and (2) after shearing and reconsolidation events. As described previously, bender-extender elements were also used to transmit and receive compression waves to assess specimen saturation before shearing events using V_p. Compression waves were transmitted, received, and interpreted using a similar process as shear waves; however, elements were excited differently by adjusting sensor wiring.

Undrained Cyclic Shearing

Undrained cyclic shearing events were performed under equivalent undrained (constant volume) conditions with no pore-pressure measurements. Cycles were stress-controlled and involved application of cyclic stress ratios ($\mathrm{CSR} = \tau/\sigma'_{v\,\mathrm{initial}}$) of 0.1, 0.15, 0.2, 0.25, and 0.3. The loading was applied at a frequency of 0.05 Hz for all tests with the exception of select uncemented loose specimens, wherein a lower frequency of 0.01 Hz was used to improve the ability of the DSS apparatus to achieve the intended loading. Displacement and stress measurements were recorded at a sampling frequency of 200 data points per cycle for all tests (either 2 or 10 Hz depending on applied loading frequency). All cyclic shearing events were terminated once specimens experienced a double-amplitude shear strain (DASS) of 24%.

Following the undrained cyclic shearing event, specimens were slowly recentered to back to their initial position (shear deformation ≈ 0%) while maintaining the current vertical stress after failure (≈0 kPa). Reconsolidation was completed by reapplying the initial vertical stress of 100 kPa. Vertical displacements were allowed to stabilize for 5 min before final V_s measurements were completed following shearing and reconsolidation events. Although it is acknowledged that actual postliquefaction reconsolidation behaviors cannot be fully captured in equivalent-undrained DSS tests, the reapplication of the vertical total stress in this testing program following cyclic loading was intended to interpret the potential for volume change in these materials following liquefaction.

Undrained Monotonic Shearing

All monotonic tests were completed under equivalent undrained (constant volume) conditions with a shearing rate of 0.022 mm/min (approximately 0.1% shear strain per minute). Shearing proceeded until all specimens achieved single-amplitude shear strains (SASS) of 24%, intended to induce a similar magnitude of damage to cemented specimens as undrained cyclic shearing events. For all tests, displacement and stress measurements were recorded at a sampling frequency of 0.5 Hz. Following monotonic shearing events, vertical effective stresses were unloaded (≈0 kPa), and specimens were slowly recentered to back to their initial positions (shear displacement ≈ 0%). Reconsolidation was completed by reapplying the initial vertical stress of 100 kPa. Vertical displacements were again allowed to stabilize for 5 min prior to V_s measurements following shearing and reconsolidation events.

$CaCO_3$ Content Measurements

Following DSS testing, soil specimens were oven-dried for at least 18 h and subsampled for $CaCO_3$ content measurements. $CaCO_3$ contents were quantified using a pressure chamber method in accordance with ASTM D4373-14 (ASTM 2014) by reacting $CaCO_3$ minerals within soil subsamples of 10–15 g with 1 M hydrochloric acid to generate CO_2 gas and a corresponding increase in test chamber pressure. Calibration relationships between generated chamber pressures and $CaCO_3$ masses were used to determine soil $CaCO_3$ contents from observed pressures. A minimum of three measurements were completed for each DSS specimen with the average $CaCO_3$ content reported. Individual measurements for the same specimen differed by no more than 0.1% by mass, and coefficients of variation (COV) for the subsample measurements were generally less than 15%.

Scanning Electron Microscope Imaging

Scanning electron microscope (SEM) images were completed with a FEI XL830 Dual-Beam Focused Ion Beam Scanning Electron Microscope (FEI Company, Hillsboro, Oregon) using an acceleration voltage of 1 kV and magnifications of 200× and 500×. Prior to imaging, soil specimens were oven-dried for an additional 2 days, mounted to imaging pedestals using carbon tape, and sputter-coated using a 60%/40% Au/Pd alloy.

Results

Summary of Undrained Cyclic Tests

Undrained cyclic tests were performed on loose biocemented specimens as well as uncemented specimens prepared to different initial D_r values. Table 1 summarizes the results of all uncemented undrained cyclic tests including specimen initial properties (e.g., packing, initial D_r, and initial V_s), applied loading ($\mathrm{CSR} = \tau/\sigma'_{v\,\mathrm{initial}}$), pretriggering results [e.g., cycles to excess pore-water pressure ratios ($r_u = \Delta u/\sigma'_{v\,\mathrm{initial}}$) of 0.475 and 0.95, and cycles to 3% SASS],

Table 1. Summary of uncemented undrained cyclic test results

Specimen initial properties[a]				Pretriggering results			Post-triggering results				
Packing[b]	D_r initial (%)	V_s initial (m/s)[c]	Loading CSR	Cycles to $r_u = 0.475$	Cycles to $r_u = 0.95$	Cycles to 3% SASS	Cycles to 5% SASS	Cycles to 9% SASS[d]	Cycles to 24% DASS[d]	Reconsolidation strain (%)[e]	ΔV_s after shearing and reconsolidation (m/s)
L	27.1	152	0.1	14.27	17.01	16.77	17.13	17.66	19.16	1.74	1
L	28.1	150	0.1	18.95	23.51	23.19	23.62	24.22	25.61	2.54	14
L	30.8	153	0.1	16.22	20.51	20.59	20.67	21.66	23.17	2.59	12
M	50.1	162	0.1	32.02	45.01	45.60	46.61	48.72	52.75	2.08	—
M	55.1	155	0.1	15.08	20.02	20.59	21.60	24.65	29.28	1.86	−13
D	73.4	167	0.1	21.93	33.01	35.72	41.71	62.21	115.73	1.83	−3
D	73.9	173	0.1	37.16	58.02	63.18	71.20	107.22	N/A	1.94	−26
D	82.1	—	0.1	64.02	96.53	104.23	119.24	204.21	N/A	1.60	—
L	28.4	137	0.15	0.76	0.99	0.77	0.80	0.80	1.14	2.30	3
L	29.9	139	0.15	0.46	1.02	0.65	0.66	1.22	2.21	2.37	−3
L	33.5	—	0.15	0.74	0.99	0.75	0.76	0.78	1.60	2.64	—
M	56.1	143	0.15	1.73	3.01	2.69	3.64	6.66	N/A	1.78	−5
M	58.4	157	0.15	2.09	3.51	3.66	5.62	10.74	18.27	1.80	−11
D	75.4	163	0.15	2.86	5.03	7.68	22.23	80.20	174.25	1.43	−12
D	79.4	—	0.15	3.96	6.52	10.21	35.24	N/A	N/A	1.28	—
L	25.5	151	0.2	0.17	0.51	0.19	0.19	0.19	0.63	2.44	−4
L	32.8	—	0.2	0.17	0.50	0.18	0.18	0.17	1.06	2.61	—
L	34.7	139	0.2	0.25	0.50	0.26	0.26	0.57	1.06	2.44	7
M	43.8	142	0.2	0.21	0.52	0.25	0.60	1.58	2.18	2.31	18
M	48.0	—	0.2	0.60	1.01	0.65	0.69	1.62	3.12	2.22	—
D	70.0	—	0.2	0.65	2.02	2.65	6.21	29.24	N/A	1.74	—
D	77.1	167	0.2	0.69	2.01	3.14	6.21	18.20	49.24	1.70	−5
L	29.7	142	0.25	0.15	0.51	0.15	0.15	0.16	0.61	2.20	3
L	29.0	133	0.25	0.15	0.50	0.15	0.16	0.17	0.58	2.42	13
M	52.5	164	0.25	0.18	0.53	0.20	0.64	1.65	3.16	2.03	−12
M	63.8	162	0.25	0.38	1.01	0.56	1.58	3.67	7.68	1.57	−18
D	78.2	171	0.25	0.38	1.02	1.69	6.22	43.25	N/A	1.50	−33
D	78.8	167	0.25	0.46	1.02	1.61	3.74	46.25	N/A	1.33	−25
L	27.2	141	0.3	0.12	0.49	0.12	0.12	0.13	0.55	2.75	32
L	35.5	139	0.3	0.12	0.49	0.12	0.12	0.13	0.54	3.01	18
M	52.0	147	0.3	0.42	0.53	0.21	0.62	1.64	3.63	1.72	−7
M	56.2	153	0.3	0.43	1.02	0.23	0.62	1.65	3.64	1.60	−16
D	69.8	164	0.3	0.42	1.02	0.72	3.20	18.24	34.73	1.36	−15
D	76.5	160	0.3	0.47	1.52	1.71	5.70	32.22	N/A	1.70	−11

[a]All specimens were initially consolidated to $\sigma'_v = 100$ kPa.
[b]L = loose; M = medium-dense; and D = dense.
[c]V_s values are reported when bender element measurements were available.
[d]N/A denotes when 9% SASS or 24% DASS was not achievable (dense samples).
[e]All specimens were reconsolidated back to $\sigma'_v = 100$ kPa.

and post-triggering results (e.g., cycles to 5% SASS, 9% SASS, and 24%DASS, reconsolidation vertical strains, and ΔV_s changes after shearing and reconsolidation events). Uncemented loose specimens had average D_r values of 30.2% (standard deviation of 3.1%) and average initial V_s values of 143 m/s (standard deviation of 7 m/s). Uncemented medium-dense specimens had average D_r values of 53.6% (standard deviation of 5.6%) and average initial V_s values of 154 m/s (standard deviation of 8 m/s). Uncemented dense specimens had average D_r values of 75.9% (standard deviation of 3.8%) and average initial V_s values of 166 m/s (standard deviation of 4 m/s).

Table 2 summarizes the results of all biocemented undrained cyclic tests including specimen initial properties (e.g., packing, initial D_r, and initial V_s), postcementation specimen properties [e.g., ΔV_s from cementation, $CaCO_3$ content by mass, COV for $CaCO_3$ content measurements, total D_r values before shearing (including cementation contributions), and increases in total D_r values (ΔD_r) from cementation], pretriggering results (e.g., cycles to r_u of 0.475 and 0.95, and cycles to 3% SASS), and post-triggering results (e.g., cycles to 5% SASS, 9% SASS, and 24% DASS, reconsolidation vertical strains, and ΔV_s changes after shearing and reconsolidation events). All biocemented tests were completed on initially loose specimens with average initial D_r values of 31.0% (standard deviation of 3.3%) and average initial V_s values of 147 m/s (standard deviation of 8 m/s), which were similar to other uncemented loose tests. Biocemented specimens achieved total D_r increases up to 5.8% and ΔV_s increases up to 100 m/s.

Biocementation-Induced Changes in V_s, D_r, and Soil Microstructure

For all specimens, increases in biocementation were expected to result in consistent increases in soil V_s values attributed to the formation of $CaCO_3$-based cementitious bonds between soil particles. Fig. 2 presents relationships among measured ΔV_s increases, soil $CaCO_3$ contents, and cementation-induced total D_r increases for all DSS specimens (data provided in Tables 1 and 2). As shown, light levels of cementation were achieved for all biocemented sand specimens with $CaCO_3$ contents up to 0.9%, which corresponded to maximum ΔV_s increases of 100 m/s and increases in soil relative

Table 2. Summary of results from biocemented undrained cyclic tests

Specimen initial properties[a]			Postcementation specimen properties						Pretriggering results			Post-triggering results				
Packing[b]	D_r initial (%)	V_s initial (m/s)	ΔV_s from cementation (m/s)	$CaCO_3$ by mass (%)	COV for $CaCO_3$ measures (%)	Total D_r (%)	ΔD_r (%)	Loading CSR	Cycles to $r_u = 0.475$	Cycles to $r_u = 0.95$	Cycles to 3% SASS	Cycles to 5% SASS	Cycles to 9% SASS	Cycles to 24% DASS	Reconsolidation strain (%)[c]	ΔV_s after shearing and reconsolidation (m/s)
L	34.0	158	6	0.17	7	35.0	1.1	0.1	27.0	36.5	36.6	36.7	37.6	38.6	3.25	−6
L	37.1	167	14	0.13	10	37.9	0.8	0.1	66.1	85.0	85.6	85.7	86.7	87.7	2.46	−22
L	31.0	150	14	0.13	12	31.8	0.8	0.1	78.0	93.5	93.3	93.6	94.1	94.6	3.11	6
L	31.0	161	19	0.11	25	31.7	0.7	0.1	109.0	125.5	125.6	126.1	126.6	127.1	3.16	−20
L	27.3	159	35	0.46	3	30.2	2.9	0.1	1,162.2	1,236.0	1,236.7	1,237.2	1,237.7	1,238.6	2.51	−26
L	36.1	146	55	0.49	9	39.2	3.1	0.1	3,022.1	3,115.0	3,115.6	3,116.1	3,116.7	3,117.6	3.18	−64
L	34.9	140	3	0.14	28	35.8	0.9	0.15	1.2	1.5	1.2	1.2	1.2	1.6	3.02	0
L	31.2	142	10	0.20	15	32.4	1.2	0.15	5.8	7.0	6.7	6.7	7.6	8.1	2.66	1
L	29.2	148	15	0.03	52	29.4	0.2	0.15	2.7	3.0	3.1	3.1	3.2	3.7	2.57	−6
L	31.4	144	20	0.19	13	32.6	1.2	0.15	21.1	24.0	23.7	23.7	24.1	24.6	2.96	−11
L	34.3	141	50	0.44	4	37.0	2.8	0.15	39.0	44.5	44.6	44.7	45.6	46.1	3.25	−52
L	26.2	140	51	0.34	7	28.4	2.1	0.15	23.0	26.0	25.8	26.1	26.6	27.1	3.00	−37
L	27.6	151	64	0.61	1	31.5	3.8	0.15	555.0	594.5	595.7	596.7	598.6	599.6	2.44	−63
L	34.5	144	82	0.63	2	38.4	4.0	0.15	1,413.1	1,452.5	1,453.6	1,454.6	1,455.7	1,457.1	2.32	−72
L	26.8	137	92	0.72	6	31.4	4.5	0.15	1,552.1	1,575.0	1,575.6	1,576.1	1,576.7	1,577.6	2.44	−80
L	31.8	159	16	0.14	10	32.7	0.9	0.2	0.6	1.0	0.7	0.7	1.1	1.6	2.51	−18
L	29.8	146	36	0.43	10	32.5	2.7	0.2	5.9	8.0	7.2	7.7	8.6	9.6	2.30	−38
L	28.6	158	54	0.41	7	31.1	2.6	0.2	9.0	11.5	11.2	11.6	12.6	13.2	2.36	−57
L	31.2	157	77	0.51	9	34.4	3.2	0.2	42.0	47.0	47.1	47.6	48.2	49.1	2.73	−77
L	30.3	146	95	0.93	2	36.1	5.8	0.2	627.0	648.0	649.1	650.1	651.7	653.6	2.25	−87
L	30.9	135	9	0.19	22	32.1	1.2	0.25	0.2	0.5	0.2	0.2	0.2	0.6	3.34	−4
L	30.6	146	36	0.30	13	32.5	1.9	0.25	1.4	2.0	1.6	1.7	2.1	2.6	2.58	−29
L	29.1	143	70	0.38	16	31.5	2.4	0.25	2.7	3.0	2.7	2.7	3.1	3.6	2.57	−73
L	28.4	142	100	0.66	3	32.6	4.2	0.25	43.0	47.5	47.6	47.7	48.6	49.2	2.52	−92
L	37.0	144	14	0.17	9	38.1	1.1	0.3	0.2	0.5	0.3	0.3	0.3	0.6	2.93	−14
L	25.1	139	32	0.38	12	27.6	2.4	0.3	0.4	0.5	0.3	0.3	0.6	1.0	2.69	−24
L	27.9	139	64	0.45	11	30.7	2.8	0.3	2.1	3.0	2.6	2.7	3.1	3.6	2.62	−47
L	35.5	142	93	0.69	4	39.8	4.3	0.3	3.0	4.0	3.7	4.2	4.6	5.6	2.47	−94

[a]All specimens were initially consolidated to $\sigma_v' = 100$ kPa.
[b]L = loose; M = medium-dense; and D = dense.
[c]All specimens were reconsolidated back to $\sigma_v' = 100$ kPa.

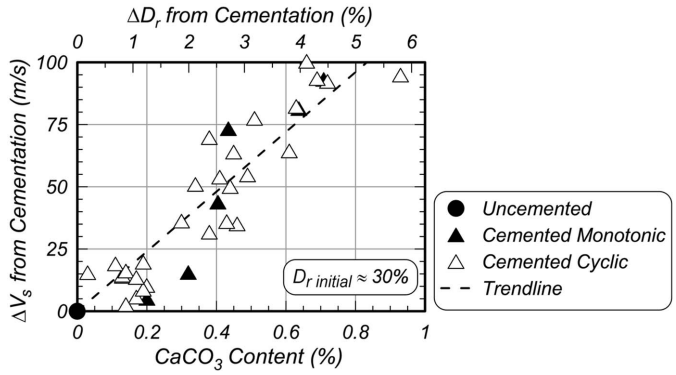

Fig. 2. Relationships among cementation-induced shear-wave velocity increases (ΔV_s), soil $CaCO_3$ contents, and changes in soil total relative densities (ΔD_r) for all biocemented and uncemented loose ($D_{r\,\text{initial}} \approx 30\%$) Ottawa F-65 specimens subjected to undrained cyclic and monotonic loading.

densities (total D_r) up to 5.8%. The near linear relationship observed between $CaCO_3$ contents and V_s increases was consistent with observations from past studies (Gomez and DeJong 2017; Gomez et al. 2018a; Darby et al. 2019; and others). The limited scatter in the relationship shown in Fig. 2 ($\approx \pm 20$ m/s ΔV_s for similar $CaCO_3$ contents) suggests that the employed biocementation processes produced similar and relatively uniform distributions of cementation on soil particle contacts and surfaces for all cementation levels considered. As expected, cementation-induced increases in soil total D_r values were relatively small, with most biocemented specimens achieving total D_r values that were within the scatter of D_r variations observed for similar uncemented loose specimens (data provided in Table 1).

Fig. 3 presents SEM images of select uncemented and biocemented sand specimens. Biocemented specimens had ΔV_s increases of 36 and 77 m/s, corresponding to $CaCO_3$ contents of 0.30% and 0.51% by mass, respectively. As shown, uncemented specimens had subrounded and rounded particles with no evidence of $CaCO_3$ crystals on soil particle surfaces [Figs. 3(a and b)]. In contrast, rhombohedral $CaCO_3$ crystals were visible on sand particle surfaces in biocemented specimens with corresponding increases in crystal frequencies observed with increases in cementation [Figs. 3(c–e)].

Unlike more heavily biocemented materials observed in many past studies (DeJong et al. 2006; Montoya and DeJong 2015; Feng and Montoya 2016; Gomez et al. 2018a; and others), these light levels of cementation did not noticeably coat soil particle surfaces with $CaCO_3$ precipitates, suggesting that particle surface roughnesses were not likely significantly altered. Collectively, these results along with those presented in Fig. 2, which showed limited densification, suggested that the dominant improvement mechanism present in the lightly biocemented specimens was $CaCO_3$ bonding between soil particles.

Effect of Biocementation on Pretriggering Behaviors

Fig. 4 presents representative undrained cyclic responses for loose specimens with varying levels of biocementation ($\Delta V_s = 0$, 16, 36, 54, 77, and 95 m/s) subjected to an applied CSR of 0.2. Figs. 4(a–f) present responses in order of increasing cementation magnitude where the first column presents shear stress versus vertical effective stress, the second column presents shear stress versus shear strain, the third column presents shear stress versus cycle number, and the fourth column presents r_u versus cycle number.

As specimens achieved higher magnitudes of cementation, as indicated by larger ΔV_s increases, dramatic increases in the number of cycles required to trigger liquefaction (criteria of either 3% SASS or $r_u = 0.95$) were observed. For example, although the uncemented specimen [Fig. 4(a)] achieved a SASS of 3% after 0.2 cycles and a r_u of 0.95 after 0.5 cycles, the most significantly biocemented specimen with a ΔV_s of 95 m/s [Fig. 4(f)] required 649 and 648 cycles to achieve a SASS of 3% and r_u of 0.95, respectively. For biocemented specimens with ΔV_s values exceeding 77 m/s, some initial dilation was also observed upon initiation of shearing [Figs. 4 (e and f)], in contrast to the immediate contractive behaviors exhibited by more weakly cemented and uncemented loose specimens.

Despite these significant improvements in liquefaction triggering resistances, all lightly biocemented specimens exhibited post-triggering behaviors that were much more similar to uncemented specimens; only 0.4 cycles were required to accumulate strains from 3% SASS to 24% DASS in the uncemented specimen, and in even the most significantly biocemented specimen ($\Delta V_s = 95$ m/s) only 4.5 cycles were required to accumulate similar strains. Furthermore, no significant changes in specimen failure envelopes were observed with increases in cementation (first column). For example, although the failure envelope for the uncemented specimen appeared to have a friction angle near 29.1°, friction angles for biocemented specimens ranged from 29.2° to 31.9° with no consistent trends observed with cementation level.

Fig. 5 presents cycles to different r_u thresholds as a function of ΔV_s increases [Figs. 5(a–c)] and total D_r values [Figs. 5(d–f)] to explore the effect of biocementation magnitudes and relative density differences on excess pore-pressure generation prior to liquefaction triggering (e.g., $r_u = 0.95$). Figs. 5(a–c) present the number of cycles needed to generate r_u of 0.475, the number of cycles needed to increase r_u from 0.475 to 0.95, and the ratio between these two values versus ΔV_s increases for all loose specimens of varying biocementation levels. Figs. 5(d–f) present similar plots versus total D_r for all biocemented specimens and uncemented specimens prepared to different initial D_r values.

As shown, pretriggering excess pore-pressure generation was evaluated in two equal increments, wherein the number of cycles needed to generate r_u of 0.475 and increase r_u from 0.475 to 0.95 represented the first and second half of excess pore-pressure generation prior to triggering, respectively. As shown, significant increases in both the number of cycles required to generate a r_u of 0.475 and to increase r_u from 0.475 to 0.95 were observed with increases in biocementation [Figs. 5(a and b)]. In addition, for almost all specimens, more cycles were required to generate r_u of 0.475 than to increase r_u from 0.475 to 0.95, with more significant differences observed for specimens subjected to lower applied CSRs [Fig. 5(c)]. Although this trend was expected due to the presence of lower effective stresses, and thus lower soil shear stiffnesses at higher excess pore pressures near triggering, more significant differences between the cycles required to generate r_u of 0.475 and the cycles required to increase r_u from 0.475 to 0.95 were observed with increases in biocementation when compared with similar uncemented specimens.

For example, whereas ratios between these cycle values were less than 5 for all uncemented specimens, these ratios appeared to consistently increase with biocementation magnitudes, reaching values near 70 at ΔV_s increases near 100 m/s [Fig. 5(c)]. This suggested that although uncemented specimens required fewer cycles to trigger liquefaction, pore pressures generated per cycle of loading were relatively similar for most cycles prior to triggering (i.e., cycles up to r_u of 0.95). In contrast, biocemented specimens appeared to require significantly more cycles during the first half of pretriggering excess pore-pressure generation (r_u of 0.475) when compared with the second half (r_u from 0.475 to 0.95). This behavior likely results

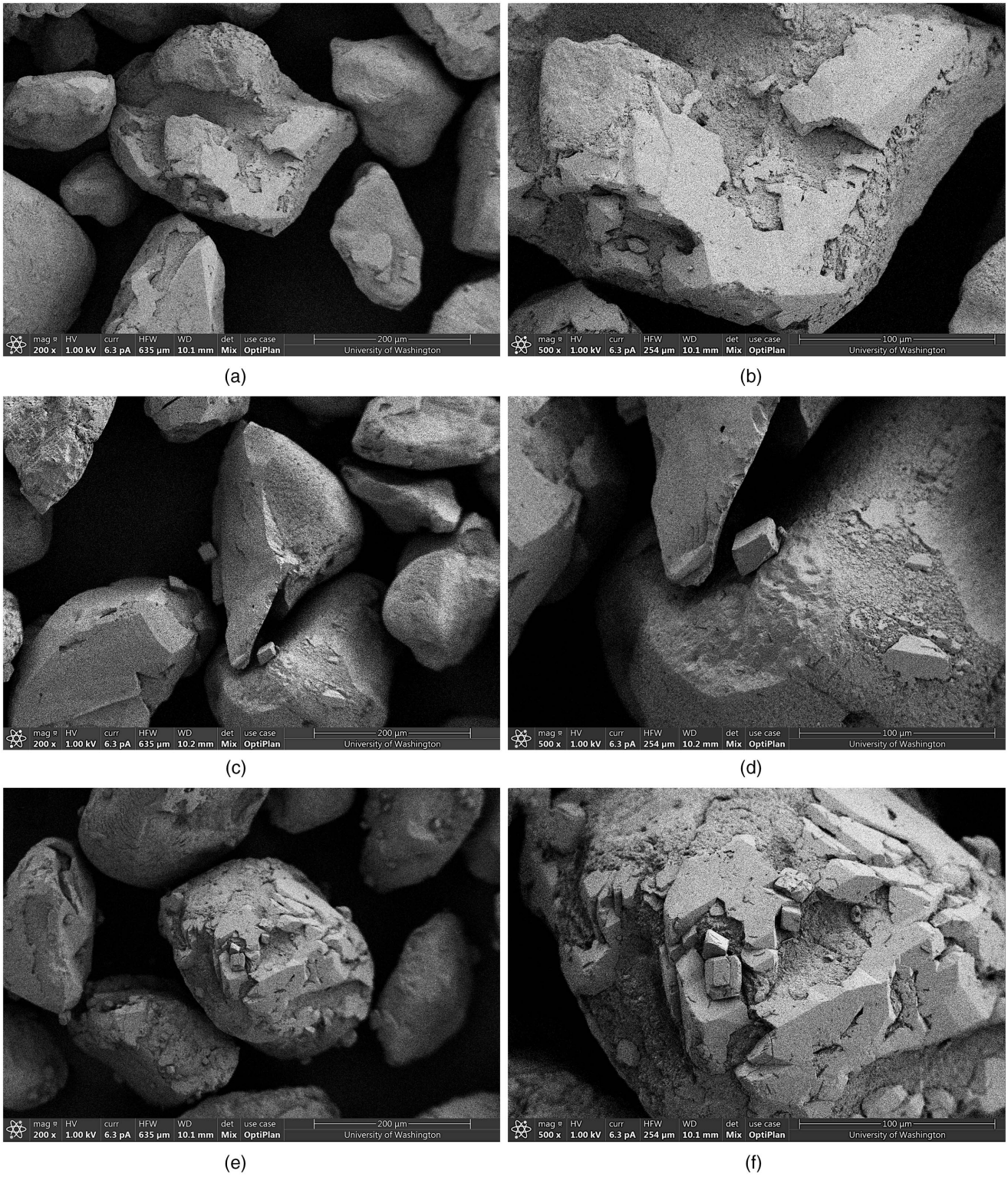

Fig. 3. SEM images of (a and b) untreated Ottawa F-65 sand and biocemented Ottawa F-65 sand specimens with ΔV_s increases of (c and d) 36 m/s; and (e and f) 77 m/s.

from the presence of lightly cemented bonds, which hold particles together and inhibit the generation of excess pore pressure at small strains during the start of cyclic loading, but become less effective at inhibiting excess pore-pressure generation as they gradually degrade with increases in strain magnitudes during later cycles.

Although biocementation appeared to significantly influence pre-triggering excess pore-pressure generation, the same conclusion cannot be drawn when examining D_r changes for uncemented specimens, where the effects observed were more limited. Although modest increases in both the number of cycles needed to generate r_u of 0.475 and to increase r_u from 0.475 to 0.95 were observed with increases in D_r for uncemented specimens [Figs. 5(d and e)], the ratios between these cycle values were again less than 5 for all uncemented tests, regardless of total D_r [Fig. 5(f)], suggesting that D_r

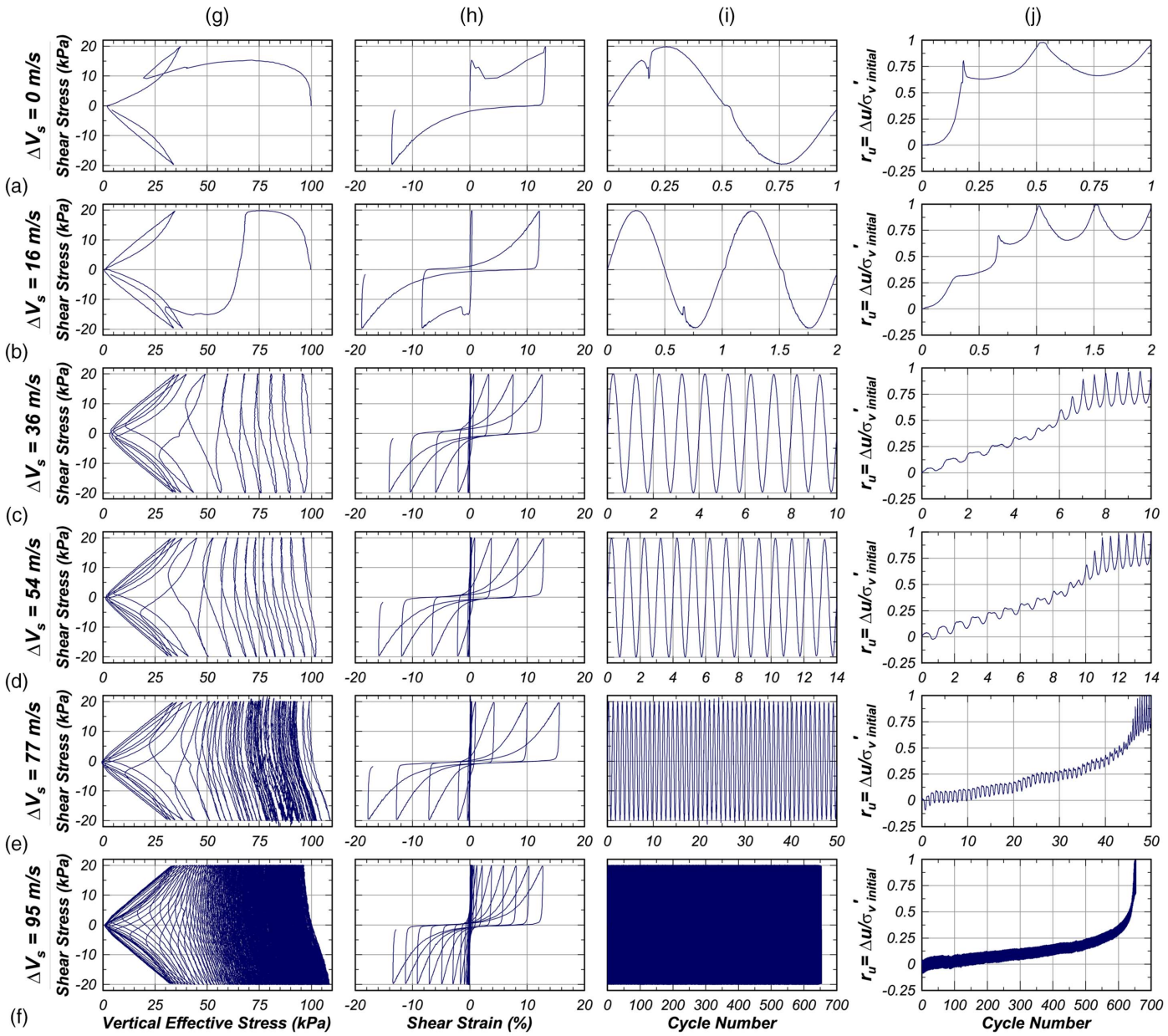

Fig. 4. Results from undrained cyclic DSS tests performed on loose ($D_{r\,\text{initial}} \approx 30\%$) Ottawa F-65 specimens of varying cementation levels (assessed by ΔV_s) subjected to a CSR of 0.2: (a) $\Delta V_s = 0$ m/s; (b) $\Delta V_s = 16$ m/s; (c) $\Delta V_s = 36$ m/s; (d) $\Delta V_s = 54$ m/s; (e) $\Delta V_s = 77$ m/s; (f) $\Delta V_s = 95$ m/s; (g) shear stress versus vertical effective stress; (h) shear stress versus shear strain; (i) shear stress versus cycle number; and (j) r_u ($=\Delta u/\sigma'_{v\,\text{initial}}$) versus cycle number.

changes alone had relatively insignificant effects on pretriggering excess pore-pressure generation.

Relationships between excess pore-pressure generation and developed shear strains were explored in order to further examine the effect of biocementation on soil pretriggering response, as well as the associated progressive destructuration of bonds during shearing. Fig. 6 presents maximum excess pore-water pressure ratios (r_u) that specimens experienced prior to first achieving a given shear strain magnitude for loose specimens of varying biocementation levels subjected to a CSR of 0.2. All shear strains are presented as absolute values; thus, information about cycle numbers and stress reversals is not shown. The provided data are representative of similar trends observed for other biocemented specimens at different applied CSRs.

As shown in Fig. 6(a), prior to triggering, biocemented specimens developed significantly smaller shear strains than uncemented specimens at similar maximum r_u values. For example, once specimens experienced a maximum r_u value near 0.6, the uncemented specimen developed shear strains near 1.5%, and the biocemented specimen with the largest increase in V_s ($\Delta V_s = 95$ m/s) experienced shear strains of only 0.25%. In addition, whereas the uncemented specimen appeared to exhibit measurable shear strains once r_u values increased above ≈0.05, biocemented specimens appeared to require significantly larger maximum r_u values exceeding ≈0.4 before shear strains greater than 0.15% were observed.

Threshold r_u values, or r_u values after which further increases in r_u resulted in large increases in shear strains, also appeared to systematically track with increases in biocementation levels.

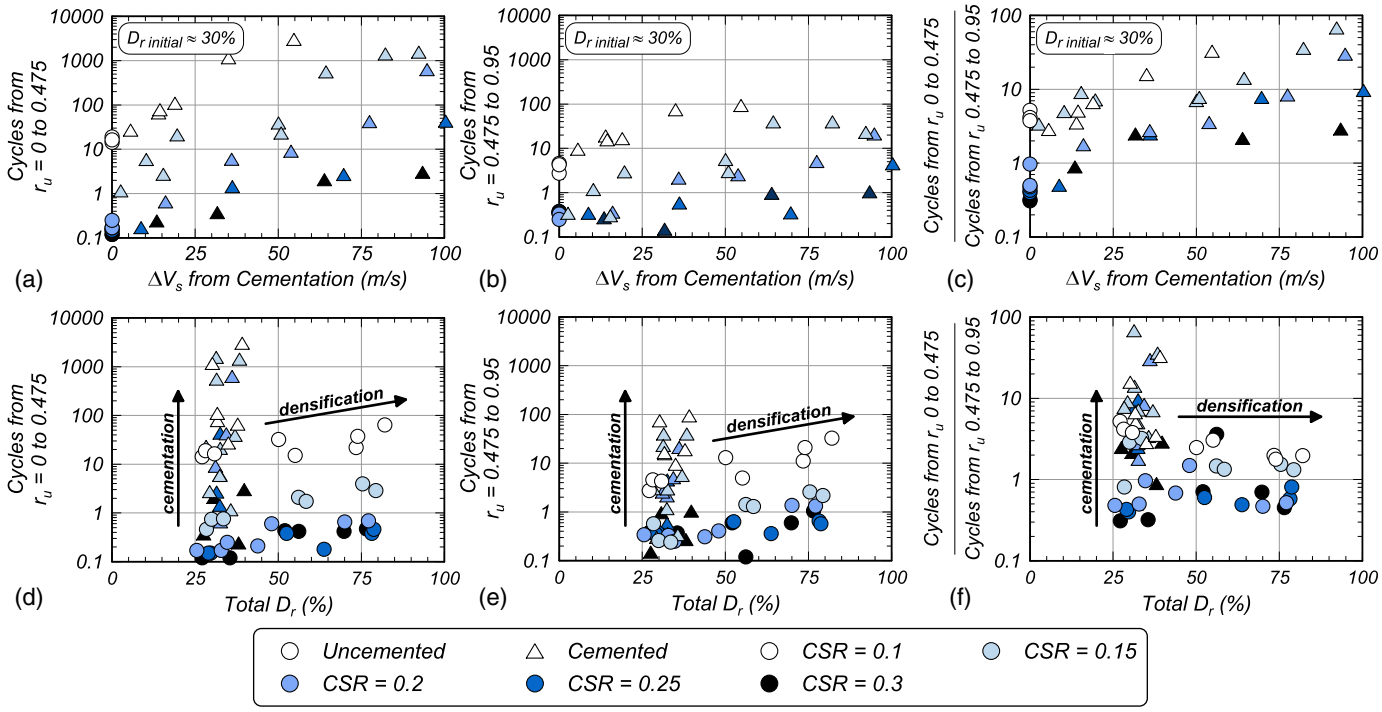

Fig. 5. Number of cycles from (a) $r_u = 0$ to 0.475; (b) $r_u = 0.475$ to 0.95; (c) ratio of (cycles from $r_u = 0$ to 0.475/cycles from $r_u = 0.475$ to 0.95) versus ΔV_s from cementation for loose ($D_{r\,\text{initial}} \approx 30\%$) biocemented specimens; number of cycles (d) from $r_u = 0$ to 0.475; (e) from $r_u = 0.475$ to 0.95; and (f) ratio of (cycles from $r_u = 0$ to 0.475/cycles from $r_u = 0.475$ to 0.95) versus total D_r for all biocemented and uncemented specimens with varying relative densities.

For example, whereas the $\Delta V_s = 36$ m/s specimen had a threshold r_u near 0.4, the $\Delta V_s = 95$ m/s specimen had a larger threshold r_u closer to 0.55. Interestingly, at larger shear strains post-triggering (>5%), biocemented specimens appeared to experience larger r_u values than uncemented specimens for similar shear strains [Fig. 6(b)]. It is hypothesized, however, that this result may be simply an artifact of the more rapid shear strain development that occurred in uncemented specimens, in contrast to biocemented specimens, wherein many more cycles were required to generate such strains, which allowed for accompanying r_u increases to more fully develop.

Collectively, these trends suggest that biocemented specimens can tolerate higher maximum excess pore-water pressure ratios (i.e., lower vertical effective stresses) than uncemented specimens before significant shear strains develop, with threshold r_u values proportional to cementation level. This behavior likely results from the presence of cemented bonds in biocemented specimens, which provide tensile strength and allow for higher soil shear stiffnesses to be maintained with increases in r_u, thus preventing shear strain development. However, it appears as though once biocemented specimens experience vertical effective stresses below some critical value (at some threshold r_u), the gradual breakage of cemented bonds intensifies, and bonds become insufficient toward preventing shear deformations, resulting in abrupt increases in shear strains and further mobilization of soil contractive volumetric tendencies, thus increasing r_u.

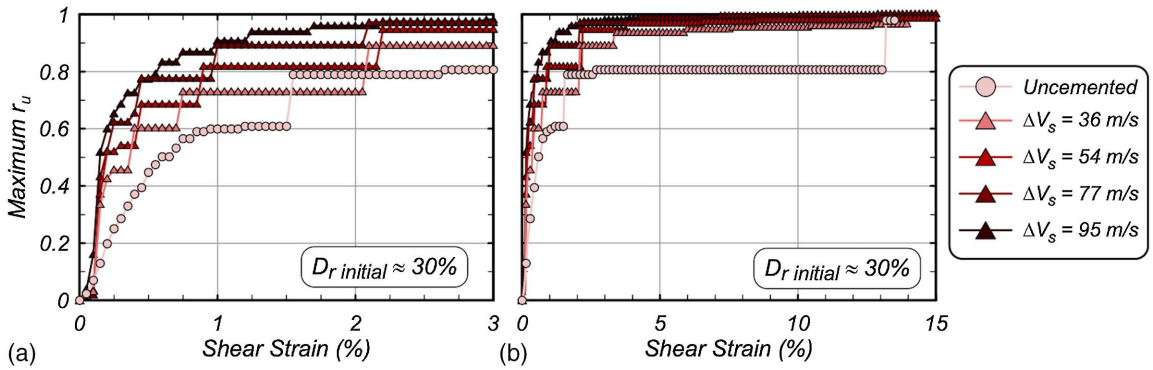

Fig. 6. Evolution of maximum excess pore-pressure ratios ($r_u = \Delta u/\sigma'_{v\,\text{initial}}$) with shear strain for loose specimens of varying cementation levels subjected to a CSR of 0.2, wherein the maximum excess pore-pressure ratio (r_u) is the largest r_u value that a specimen has experienced prior to achieving different shear strains. Plots present similar data for shear strains from 0% to (a) 3%; and (b) 15%. Data points were evaluated at discrete increments of 0.05% shear strain.

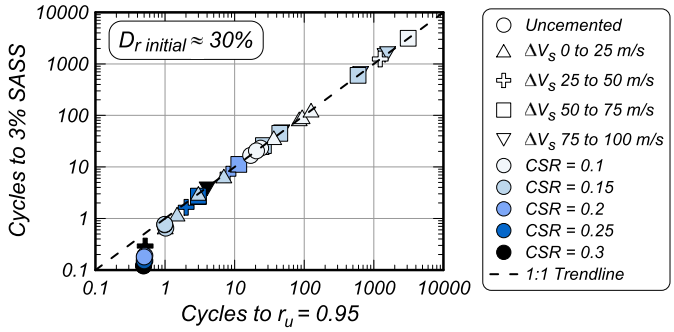

Fig. 7. Number of cycles to 3% SASS versus number of cycles to $r_u = 0.95$ for specimens of varying biocementation (indicated by ΔV_s) subjected to different applied CSRs. A 1:1 trendline is provided to compare criteria.

Established liquefaction triggering criteria were employed in order to examine changes in soil liquefaction triggering resistances with changes in biocementation levels, D_r, and applied loading magnitudes. The two liquefaction triggering criteria considered were (1) number of loading cycles required to achieve a SASS of 3% (Ishihara 1993), and (2) number of loading cycles required to achieve a r_u of 0.95 (Ishihara 1993; Wu et al. 2004). A criterion of $r_u = 0.95$ was used instead of $r_u = 1.0$ to account for potential variations in laboratory measurements, as recommended by Wu et al. (2004). Fig. 7 presents relationships between the number of loading cycles required to achieve SASS of 3% and the number of loading cycles required to achieve r_u of 0.95 for all loose specimens of varying biocementation levels subjected to different applied loading magnitudes.

As shown, both liquefaction triggering criteria yielded nearly identical results, with almost all specimens following a 1:1 trend. Results between criteria diverged only slightly for specimens subjected to higher CSR values (>0.2) when triggering occurred within less than one cycle for both approaches. Because no significant differences were observed between criteria and all tests were completed under equivalent-undrained conditions with no direct pore-pressure measurements, the number of loading cycles to 3% SASS was used to evaluate liquefaction triggering for all further results presented in this study.

Fig. 8 presents relationships between the number of cycles to 3% SASS versus ΔV_s from cementation [Fig. 8(a)], soil $CaCO_3$ contents [Fig. 8(b)], and total D_r values [Fig. 8(c)]. As mentioned previously, all biocemented specimens shown in Figs. 8(a and b) had similar initial D_r values near 30%. For all CSR magnitudes, increases in biocementation, as indicated by V_s and $CaCO_3$ content increases, resulted in log-linear increases in the number of cycles required to trigger liquefaction, with the most pronounced effects at low CSR values [Figs. 8(a and b)].

For example, as ΔV_s values increased from 0 m/s (uncemented) to 50 m/s, cycles to trigger liquefaction increased by nearly 2 orders of magnitude for CSR of 0.1, 0.15, and 0.2 specimens, respectively; however, cycles to trigger liquefaction increased by a significant but smaller 1–1.5 orders of magnitude for specimens at CSRs exceeding 0.25. At higher levels of biocementation near a ΔV_s of 100 m/s, tests could only be performed at CSR values exceeding 0.15, and results suggested improvements in the cycles to trigger liquefaction between 1.5 and 3 orders of magnitude when compared with similar uncemented specimens. When comparing ΔV_s-based [Fig. 8(a)] and $CaCO_3$ content–based [Fig. 8(b)] relationships, similar trends were observed; however, noticeably larger scatter was observed in the $CaCO_3$ content–based relationship. As discussed previously, even when identical cementation treatment techniques are used, variations in ΔV_s increases can occur at the same $CaCO_3$ content (Fig. 2) as a result of small differences in the distribution of biocementation on particle surfaces and contacts. The better correlation between the number of cycles to liquefaction triggering and ΔV_s suggests that V_s measurements may offer improved assessment of triggering behaviors when compared with mass-based quantification of biocementation.

Fig. 8(c) provides the relationship between number of cycles to trigger liquefaction (3% SASS) and total D_r for all biocemented loose specimens as well as uncemented specimens prepared to different initial D_r values (≈30%–75%). It should be mentioned that total D_r variations for cemented specimens are again indicative of both small differences in initial preparation and small dry-density increases resulting from biocementation. As shown for uncemented specimens, when soil D_r values increased, increases in the number of cycles to trigger liquefaction were also observed; however, improvements were not as significant as those obtained with increases in biocementation. For example, when D_r values increased from ≈30% to 75% for uncemented specimens subjected to a CSR of 0.1, increases in the number of cycles to trigger liquefaction of less than 1 order of magnitude was observed. When compared with loose biocemented specimens (under the same applied CSR of 0.1), however, a ΔV_s increase of only 19 m/s would be needed to achieve similar improvement.

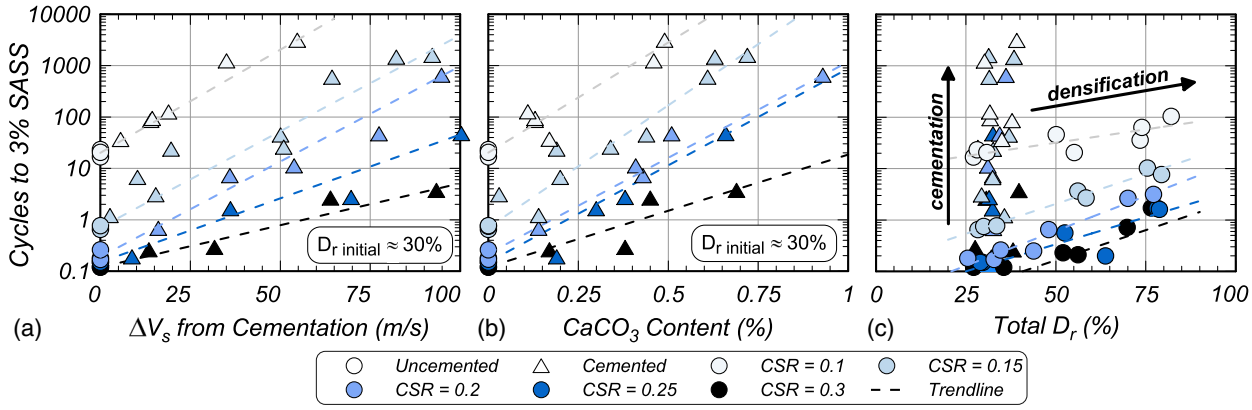

Fig. 8. Number of cycles to 3% SASS versus (a) ΔV_s from biocementation; (b) $CaCO_3$ contents for loose ($D_{r\,initial} \approx 30\%$) specimens of varying biocementation; and (c) number of cycles to 3% SASS versus total relative densities (D_r) for all biocemented and uncemented specimens of varying D_r.

J. Geotech. Geoenviron. Eng., 2022, 148(1): 04021170

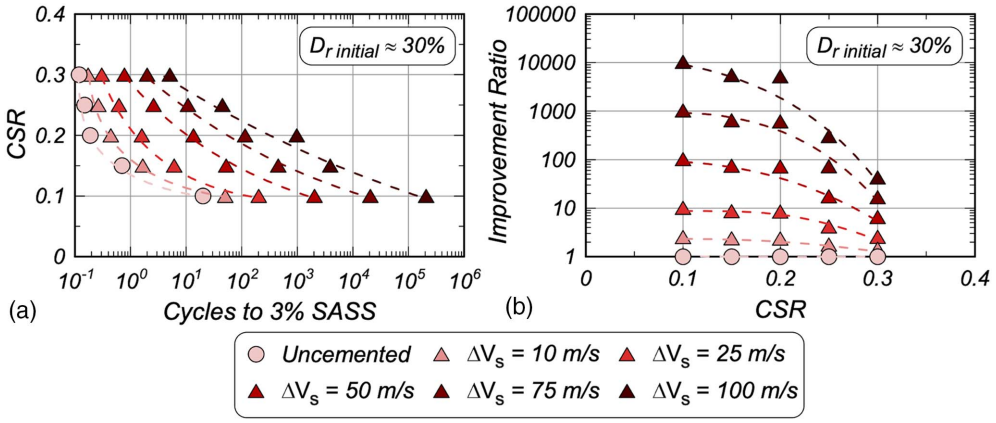

Fig. 9. Relationships between (a) applied CSRs versus number of cycles to 3% SASS; and (b) improvement ratios ($N_{3\%\,\text{SASS Cemented}}/N_{3\%\,\text{SASS Uncemented}}$) versus applied CSRs for loose ($D_{r\,\text{initial}} \approx 30\%$) specimens of varying biocementation levels ($\Delta V_s = 0$, 10, 25, 50, 75, and 100 m/s).

These results may have significant practical implications because densification of loose soils via various ground-improvement techniques (e.g., deep dynamic compaction) is oftentimes considered for liquefaction mitigation. Although soil densification did yield modest improvements in liquefaction triggering resistances, for the loading magnitudes considered in this study, the presence of light levels of biocementation resulted in more dramatic improvements in liquefaction triggering behaviors.

Fig. 9 presents relationships between applied CSRs versus number of cycles to trigger liquefaction (3% SASS) [Fig. 9(a)] and improvement ratios versus applied CSRs [Fig. 9(b)] for varying biocementation levels. Improvement ratios were determined by dividing the number of cycles needed to achieve 3% SASS in biocemented specimens by that required for identical uncemented specimens. Because biocemented specimens with identical ΔV_s values were not tested at different CSR values, and the number of cycles to liquefaction triggering was shown to change dramatically with even small increases in ΔV_s, trendline relationships between ΔV_s values and number of cycles to 3% SASS presented in Fig. 8(a) were used to develop curves by estimating cycles to 3% SASS for consistent ΔV_s increments.

As shown in Fig. 9(a), developed curves allow for changes in liquefaction resistances with changes in applied CSRs to be understood for a single cementation level (i.e., ΔV_s increase). Several main trends are observed from these liquefaction triggering curves: (1) with increases in biocementation magnitudes, increases in the number of cycles to 3% SASS occur for all applied CSRs, and (2) the effect of biocementation on soil liquefaction triggering resistances was more pronounced at lower applied CSRs than at higher CSRs. Similar trends can be observed in Fig. 9(b), where improvement ratios are largest with increasing biocementation at lower applied CSRs. For example, the highest cementation level considered ($\Delta V_s = 100$ m/s) had an improvement ratio of 10,363 at a CSR of 0.1; however, this same cementation level corresponded to an improvement ratio of only 43 at a CSR of 0.3.

Although changes in cyclic resistances with applied loading magnitudes are expected even for uncemented soils (Idriss and Boulanger 2008), these resistances appeared to be more significantly influenced by applied loading magnitudes with increases in biocementation. It is hypothesized that the greater improvement ratios observed at lower CSRs are related to the mode of cemented bond destructuration, which involves more gradual fatigue-like deterioration at smaller applied CSRs, in comparison with more abrupt damage of cemented bonds at higher applied CSRs. A power-law function is commonly used to describe the functional form of liquefaction triggering curves (e.g., $\text{CSR} = a \times N_L^b$, wherein N_L is number of cycles to 3% SASS, and a and b values are empirically fit parameters that capture the vertical position and slope of curves, respectively). However, this functional form did not appear to reasonably capture observed trends for biocemented specimens in this study. Significant discrepancies have also been reported between past studies, wherein the slopes of liquefaction triggering curves (i.e., b values) have been suggested to decrease (Hernandez 2018; Xiao et al. 2018, 2019a), remain constant, or even increase (Riveros and Sadrekarimi 2020) with increasing biocementation, suggesting that further investigation of this aspect is needed.

Effect of Biocementation on Post-Triggering Behaviors

Numbers of cycles to different strain thresholds following triggering were examined in order to explore changes in post-triggering behaviors with changes in biocementation magnitudes and relative densities. Fig. 10 presents the number of cycles from 3% to 9% SASS versus ΔV_s from cementation [Fig. 10(a)], the number of cycles from 3% to 9% SASS versus total D_r [Fig. 10(b)], and the number of cycles from 3% SASS to 24% DASS versus ΔV_s from cementation [Fig. 10(c)].

As shown in Figs. 10(a and c), for all biocementation levels and applied CSRs, almost no detectable changes in post-triggering strain-accumulation behaviors were observed when compared with the behavior of the uncemented specimens. For example, a maximum of only three additional cycles were required for biocemented specimens relative to uncemented specimens to progress from 3% to 9% SASS [Fig. 10(a)], with a maximum of only four additional cycles required to progress from 3% SASS to 24% DASS [Fig. 10(c)]. The limited improvements in post-triggering strain-accumulation behaviors with increases in biocementation suggest that biocemented bonds may be already significantly damaged prior to triggering, with the effect of light cementation diminished at larger strains due to the absence of cohesive bonds and the limited densification of specimens ($\Delta D_r < 5.8\%$).

In contrast, when the post-triggering behavior of uncemented specimens prepared to different D_r values was compared with that of biocemented loose specimens, significant differences were observed [Fig. 10(b)]. For example, when the D_r of uncemented specimens was increased from ≈30% to 75%, the number of cycles

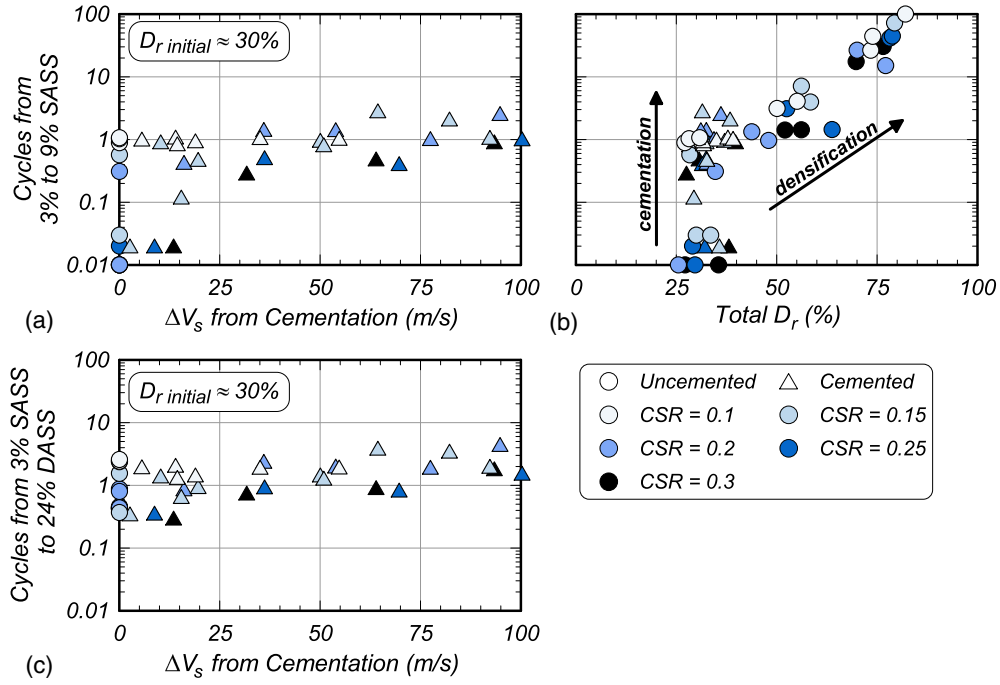

Fig. 10. Number of cycles from 3% to 9% SASS versus (a) ΔV_s from cementation for loose ($D_{r\,\text{initial}} \approx 30\%$) specimens of varying biocementation; (b) D_r for all biocemented specimens and uncemented specimens prepared at varying D_r; and (c) number of cycles from 3% SASS to 24% DASS versus ΔV_s from cementation for loose ($D_{r\,\text{initial}} \approx 30\%$) specimens of varying biocementation.

from 3% to 9% SASS increased by over two orders of magnitude for all applied CSRs [Fig. 10(b)]. Large improvements in post-triggering strain-accumulation behaviors with increases in soil D_r were in stark contrast to the minimal effects of light biocementation and resulted from increasingly dilative volumetric behaviors (Bolton 1986). Interestingly, when compared on the basis of total D_r, results from biocemented and uncemented specimens were relatively consistent [Fig. 10(b)], further suggesting that light biocementation may have minimal effects on soil post-triggering shearing behaviors beyond those afforded by small dry-density increases.

In addition to strain accumulation, changes in reconsolidation behaviors following shearing events were also examined with changes in soil biocementation levels and D_r. Fig. 11 presents reconsolidation strains versus ΔV_s from cementation for all biocemented loose specimens [Fig. 11(a)] as well as D_r for all biocemented loose specimens and uncemented specimens prepared to varying initial D_r values [Fig. 11(b)]. Reconsolidation vertical strains were measured during the reapplication of the 100-kPa vertical effective stress following the accumulation of 24% DASS for all samples.

As shown in Fig. 11(a), as biocementation magnitudes increased, almost no effects on reconsolidation strains were observed. For example, for biocemented specimens with ΔV_s values near 100 m/s, average reconsolidation strains were reduced by only 1.65% (0.04% strain) when compared with uncemented specimens. In several instances, reconsolidation strains for biocemented specimens with ΔV_s increases of less than 50 m/s even exceeded those for similar uncemented specimens. In contrast, soil D_r increases were observed to have much more dramatic effects on reconsolidation behaviors, with average reconsolidation strains decreasing by nearly 36% (0.88% strain) for uncemented specimens when D_r was increased from ≈30% to 75% [Fig. 11(b)]. Reconsolidation trends were consistent with previous post-triggering strain-accumulation behaviors and again suggested that light levels of biocementation ($\Delta V_s < 100$ m/s) may afford almost no improvements in large-strain soil behaviors.

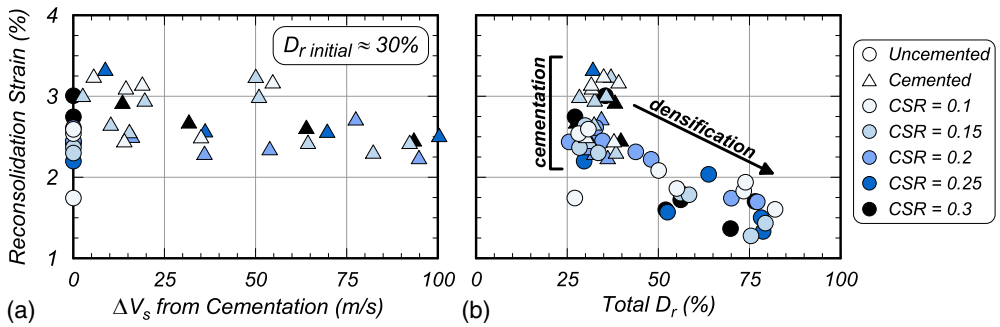

Fig. 11. Reconsolidation strains versus (a) ΔV_s from cementation for loose ($D_{r\,\text{initial}} \approx 30\%$) specimens of varying biocementation levels; and (b) total D_r for all biocemented loose specimens and uncemented specimens prepared at varying initial D_r.

J. Geotech. Geoenviron. Eng., 2022, 148(1): 04021170

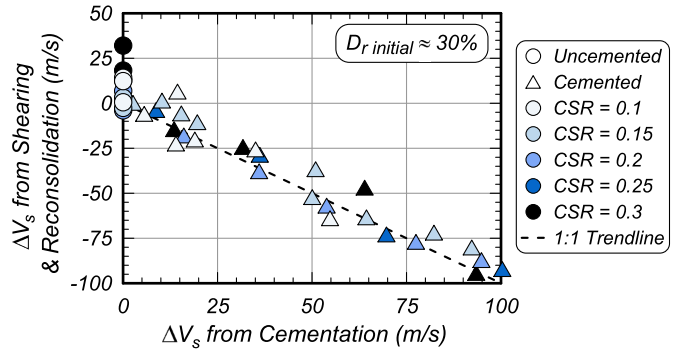

Fig. 12. Shear-wave velocity changes (ΔV_s) following shearing and reconsolidation events versus shear-wave velocity increases (ΔV_s) from cementation for loose ($D_{r\,\text{initial}} \approx 30\%$) specimens of varying cementation with different applied CSRs. Data points plotting near the 1:1 trendline suggest that increases in V_s from cementation were eliminated following shearing and reconsolidation events.

Fig. 12 presents relationships between ΔV_s changes measured following shearing and reconsolidation events and ΔV_s increases resulting from biocementation. The ΔV_s changes measured following shearing and reconsolidation were indicative of both V_s decreases resulting from biocementation damage during shearing events, as well as potential V_s increases resulting from soil densification during reconsolidation. For all biocemented specimens, shearing events were stopped following the accumulation of 24% DASS; thus, all specimens experienced similar shear-strain magnitudes prior to reconsolidation. For all uncemented specimens, ΔV_s increases from biocementation were nonexistent; however, following shearing and reconsolidation events, small increases in V_s values of less than 25 m/s were observed resulting from some densification.

For biocemented specimens, ΔV_s increases from cementation had similar magnitudes to ΔV_s decreases following shearing and reconsolidation events, suggesting that small-strain stiffness improvements resulting from light biocementation were largely erased following shearing events, irrespective of applied CSRs or cementation levels. Some biocemented specimens plotted above the 1:1 trendline by less than 25 m/s and may be suggestive of small V_s increases due to specimen densification and/or some retention of cementation integrity (i.e., bonding). The absence of significant ΔV_s increases from biocementation remaining following shearing events was consistent with other post-triggering observations, which suggested that light biocementation had limited effects at larger strains.

Summary of Undrained Monotonic Tests

Undrained monotonic tests were performed on loose specimens of varying biocementation levels to examine changes in stress-strain behaviors and volumetric tendencies with changes in cementation and to relate observed monotonic responses to previous cyclic results. Table 3 summarizes the results of all undrained monotonic tests, including specimen initial properties (e.g., packing, initial D_r, and initial V_s), postcementation specimen properties [e.g., ΔV_s from cementation, $CaCO_3$ content by mass, COV for $CaCO_3$ content measurements, total D_r values before shearing (including cementation contributions), and increases in total D_r values (ΔD_r) from cementation], and test results (e.g., peak shear stress from 0% to 3% SASS, corresponding CSR to achieve 3% SASS in 0.25 cycles, reconsolidation vertical strains, and ΔV_s changes after shearing and reconsolidation events). All specimens had initial D_r values between 26.4% and 33.3% and initial V_s values between 136 and 152 m/s. Biocemented specimens achieved D_r increases up to 4.5% and V_s increases up to 93 m/s, which were consistent with the light biocementation levels investigated in cyclic tests (Fig. 2).

Effect of Biocementation on Undrained Monotonic Behaviors

Fig. 13 presents results from undrained monotonic tests including shear stresses versus shear strains [Fig. 13(a)], shear stresses versus vertical effective stresses [Fig. 13(b)], and excess pore-water pressures versus shear strains [Fig. 13(c)] for loose specimens of varying biocementation levels ($\Delta V_s = 0$, 16, 44, 81, and 93 m/s).

As shown, all specimens exhibited initially contractive tendencies at strains less than 0.25%, with increasingly dilative behaviors observed at larger strains with increases in biocementation. Biocemented specimens with ΔV_s increases less than or equal to 44 m/s exhibited strong contractive volumetric tendencies, with positive excess pore-water pressures observed at all shear strains. In more significantly biocemented specimens (ΔV_s values of 81 and 93 m/s), however, dilative volumetric behaviors were observed with negative excess pore-water pressures generated at higher shear strains. Corresponding increases in vertical effective stresses in more significantly biocemented specimens resulted in increases in shear strengths and stiffnesses with increases in biocementation.

Table 3. Summary of results from undrained monotonic tests

Specimen initial properties[a]			Postcementation specimen properties					Results			
Packing[b]	D_r initial (%)	V_s initial (m/s)	ΔV_s from cementation (m/s)	$CaCO_3$ by mass (%)	COV for $CaCO_3$ measures (%)	Total D_r (%)	ΔD_r (%)	Peak τ from 0 to 3% SASS (kPa)	CSR 3% SASS in 0.25 cycles	Reconsolidation strain (%)[c]	ΔV_s after shearing and reconsolidation (m/s)
L	30.3	138	0	0.00	—	30.3	—	17.7	0.18	2.95	−2
L	33.3	139	5	0.20	35	34.6	1.3	20.0	0.20	2.82	−9
L	32.6	141	16	0.32	14	34.6	2.0	24.0	0.24	2.78	−20
L	27.5	140	44	0.40	10	30.0	2.6	30.8	0.31	2.80	−48
L	26.4	136	73	0.43	11	29.2	2.8	32.9	0.33	2.85	−74
L	28.3	152	81	0.64	9	32.3	4.0	49.1	0.49	1.41	−86
L	31.2	138	93	0.71	9	35.6	4.5	72.0	0.72	2.44	−99

[a]All specimens were initially consolidated to $\sigma_v' = 100$ kPa.
[b]L = loose; M = medium-dense; and D = dense.
[c]All specimens were reconsolidated back to $\sigma_v' = 100$ kPa.

J. Geotech. Geoenviron. Eng., 2022, 148(1): 04021170

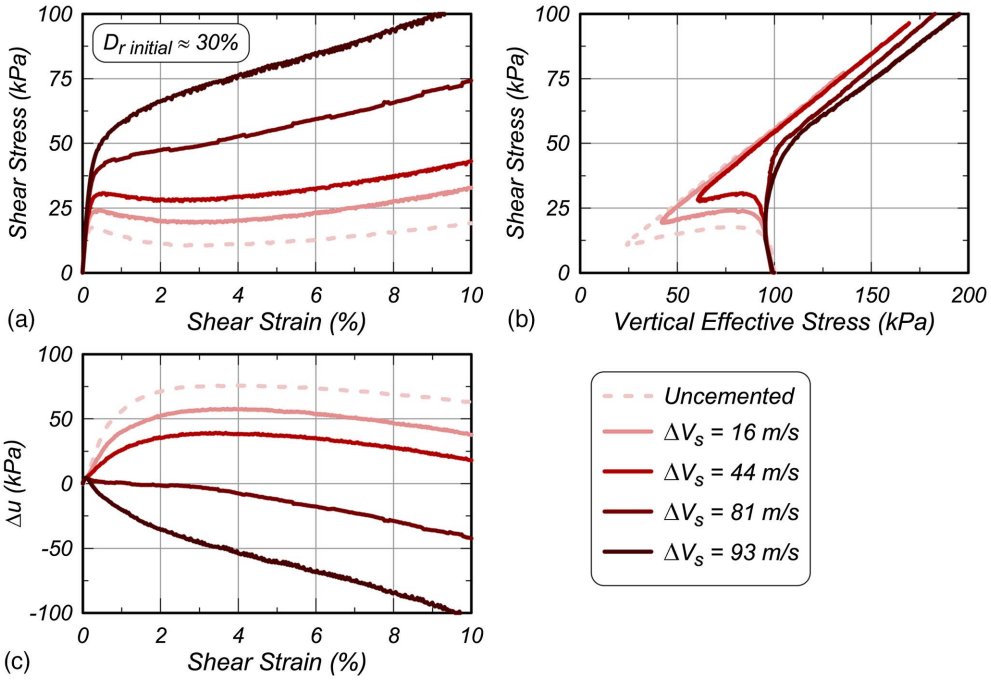

Fig. 13. Results from undrained monotonic tests on loose ($D_{r\,\text{initial}} \approx 30\%$) specimens of varying biocementation levels, including plots of (a) shear stresses versus shear strains; (b) shear stresses versus vertical effective stresses; and (c) excess pore-water pressures (Δu) versus shear strains.

Although some of these improvements may have also resulted from increases in soil cohesion and interparticle friction, only small differences in failure envelopes were observed with increases in biocementation, suggesting that observed improvements were primarily related to changes in volumetric behaviors. When comparing behaviors at shear strains of less than 3%, representative of strain magnitudes experienced in cyclic specimens prior to triggering, significant differences in peak shear strengths and stiffnesses were observed. For example, from 0% to 3% shear strain, the peak shear strength of the uncemented specimen was only 17.7 kPa, whereas the most significantly biocemented specimen (ΔV_s of 93 m/s) achieved a peak shear strength of 72 kPa, an increase of over 300%.

In order to compare observed undrained monotonic responses to pretriggering behaviors observed in undrained cyclic tests, the CSR required to achieve 3% SASS in 0.25 cycles (equivalent to triggering during undrained monotonic shearing) was determined by taking the peak shear stress observed from 0% to 3% SASS in monotonic tests (Fig. 13) and normalizing this value by the initial vertical effective stress of 100 kPa. The ΔV_s magnitudes resulting in triggering in 0.25 cycles for CSRs applied during cyclic testing were also determined from results presented in Fig. 9(a). Fig. 14 presents CSRs required to achieve 3% SASS in 0.25 cycles determined from both undrained monotonic and cyclic tests versus ΔV_s from cementation for loose specimens of varying biocementation levels.

As expected, CSRs required to trigger liquefaction in 0.25 cycles agreed well between both cyclic and monotonic tests, with CSR values increasing from near 0.2 for uncemented loose specimens to near 0.7 for biocemented loose specimens with ΔV_s values near 100 m/s. Biocemented cyclic results were only plotted up to a ΔV_s increase of 25 m/s because applied CSR values exceeding 0.3 were not investigated during cyclic tests. The observed consistency between test results suggests that the liquefaction triggering behavior of biocemented soils may be further characterized through the strategic combination of monotonic and cyclic undrained tests in future studies.

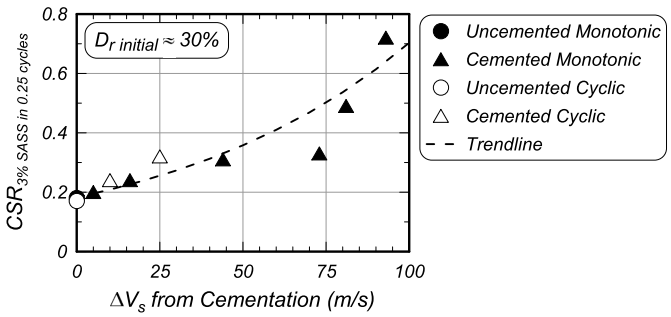

Fig. 14. Relationships between applied CSRs required to achieve 3% SASS in 0.25 cycles and ΔV_s from cementation for loose ($D_{r\,\text{initial}} \approx 30\%$) specimens of varying cementation as determined from both undrained monotonic and cyclic DSS tests.

Conclusions

A study was completed to evaluate the liquefaction triggering and post-triggering behaviors of lightly biocemented loose sands. Twenty-eight undrained cyclic DSS tests were performed on biocemented Ottawa F-65 sand specimens prepared to loose relative densities, treated to varying light biocementation levels (ΔV_s = 0–100 m/s, $CaCO_3$ contents = 0%–0.93%), and subjected to different loading magnitudes (CSR = 0.1–0.3). Thirty-four similar undrained cyclic DSS tests were also performed on uncemented specimens prepared to loose ($D_r \approx 30\%$), medium-dense ($D_r \approx 55\%$), and dense ($D_r \approx 75\%$) relative densities to compare the response of biocemented soils with behavioral improvements achievable through densification. Seven undrained monotonic tests were also performed on biocemented loose specimens to further investigate stress-strain behaviors and observations from cyclic testing.

From the results of this study, the following conclusions can be made:

- The presence of light levels of biocementation can significantly improve the pretriggering behaviors of loose sands with more limited shear strains observed with increasing r_u and significantly more cycles required to generate excess pore-water pressures initially during undrained cyclic loading.
- Light levels of biocementation can dramatically improve the liquefaction resistance of loose sands with the number of cycles required to trigger liquefaction increasing by over 3 orders of magnitude at smaller applied CSRs and higher biocementation levels ($\Delta V_s \approx 100$ m/s).
- Pretriggering improvements afforded by light biocementation ($\Delta V_s \approx 100$ m/s) exceeded those achievable through soil densification ($D_r \approx 30\%$–75%) for all loading magnitudes considered (CSR $= 0.1$–0.3).
- Pretriggering behaviors observed for biocemented specimens correlated best with increases in soil V_s rather than $CaCO_3$ contents or increases in D_r from precipitated $CaCO_3$ masses.
- In stark contrast to pretriggering behaviors, post-triggering strain-accumulation and reconsolidation behaviors were not significantly improved by the presence of light levels of biocementation, with V_s measurements suggesting that small-strain stiffness improvements afforded by light biocementation were largely erased following shearing and reconsolidation events.
- Undrained monotonic tests demonstrated that light levels of biocementation can result in large increases in shear strengths and stiffnesses through increasingly dilative volumetric tendencies with interpreted cyclic strengths that were consistent with those obtained from undrained cyclic testing.

Although the obtained results suggest that light levels of biocementation can dramatically improve soil liquefaction–triggering resistances, further investigations are needed to provide a more comprehensive understanding of these materials including potential improvements in post-triggering behaviors obtainable at higher cementation levels and the effect of various practical loading scenarios, treatment techniques, and initial soil conditions.

Data Availability Statement

All data generated during the study are available from the corresponding author upon reasonable request. All measured data presented in the figures of this paper will be available through the NSF DesignSafe-CI Data Depot repository (https://www.designsafe-ci.org/data/browser/public/) under Project No. PRJ-2912.

Acknowledgments

Support for this research provided by the University of Washington and the Engineering Research Center Program of the National Science Foundation under NSF Cooperative Agreement No. EEC-1449501 is greatly appreciated. Any opinions, findings, and conclusions or recommendations expressed in this manuscript are those of the authors and do not necessarily reflect the views of the National Science Foundation. Presented SEM images were made possible by the Molecular Analysis Facility, a National Nanotechnology Coordinated Infrastructure site at the University of Washington, which is supported in part by the National Science Foundation Grant NNCI-1542101, the University of Washington, the Molecular Engineering & Science Institute, and the Clean Energy Institute. The authors appreciate insightful discussions with Professor Jason T. DeJong, which greatly improved the study. Research assistance from Dr. Scott Braswell and Lucas Lindberg are acknowledged and appreciated.

References

Akili, W., and M. A. A.-J. Nabil. 1988. "Cone penetration tests on artificially cemented sands." In Vol. 2 of *Proc., 1st Int. Symp. on Penetration Testing*, 607–613. Rotterdam, Netherlands: A.A. Balkema.

ASTM. 2014. *Standard test method for rapid determination of carbonate content of soils*. ASTM D4373-14. West Conshohocken, PA: ASTM.

ASTM. 2016a. *Standard test methods for maximum index density and unit weight of soils using a vibratory table*. ASTM D4253-16e1. West Conshohocken, PA: ASTM.

ASTM. 2016b. *Standard test methods for minimum index density and unit weight of soils and calculation of relative density.* ASTM D4254-16. West Conshohocken, PA: ASTM.

ASTM. 2017. *Standard practice for classification of soils for engineering purpose*. ASTM D2487-17e1. West Conshohocken, PA: ASTM.

Bachus, R. C., G. W. Clough, N. Sitar, N. Shafii-Rad, J. Crosby, and P. Kaboli. 1981. *Behavior of weakly cemented soil slopes under static and seismic loading conditions, Vol. II*. USGS Rep. No. 51. Washington, DC: USGS.

Bernardi, D., J. T. DeJong, B. M. Montoya, and B. C. Martinez. 2014. "Bio-bricks: Biologically cemented sandstone bricks." *Constr. Build. Mater.* 55 (Mar): 462–469. https://doi.org/10.1016/j.conbuildmat.2014.01.019.

Bhattacharya, A., S. N. Naik, and S. K. Khare. 2018. "Harnessing the biomineralization ability of urease producing *Serratia marcescens* and *Enterobacter cloacae* EMB19 for remediation of heavy metal cadmium (II)." *J. Environ. Manage.* 215 (Jun): 143–152. https://doi.org/10.1016/j.jenvman.2018.03.055.

Bolton, M. D. 1986. "The strength and dilatancy of sands." *Géotechnique* 36 (1): 65–78. https://doi.org/10.1680/geot.1986.36.1.65.

Burdalski, R. J.II. 2020. "Investigating the effect of biological and chemical factors on the reaction kinetics and mineralogy of ureolytic biocementation." Master's thesis, Dept. of Civil and Environmental Engineering, Univ. of Washington.

Burdalski, R. J., and M. G. Gomez. 2020. "Investigating the effect of microbial activity and chemical concentrations on the mineralogy and morphology of ureolytic bio-cementation." In *Proc., Geo-Congress 2020: Biogeotechnics*, 83–95. Reston, VA: ASCE.

Carey, T. J., N. Stone, and B. L. Kutter. 2020. "Grain size analysis and maximum and minimum dry density testing of Ottawa F-65 sand for LEAP-UCD-2017." In *Model tests and numerical simulations of liquefaction and lateral spreading*, 31–44. Cham, Switzerland: Springer.

Choi, S. G., K. Wang, and J. Chu. 2016. "Properties of biocemented, fiber reinforced sand." *Constr. Build. Mater.* 120 (Sep): 623–629. https://doi.org/10.1016/j.conbuildmat.2016.05.124.

Clough, G. W., and R. C. Bachus. 1981. "An investigation of sampling disturbance in weakly cemented soils." In *Proc., Engineering Foundation Conf. in Updating Subsurface Sampling and In-situ Testing*. Reston, VA: ASCE.

Clough, G. W., J. Iwabuchi, N. S. Rad, and T. Kuppusamy. 1989. "Influence of cementation on liquefaction of sands." *J. Geotech. Eng.* 115 (8): 1102–1117. https://doi.org/10.1061/(ASCE)0733-9410(1989)115:8(1102).

Clough, G. W., N. Sitar, R. C. Bachus, and N. S. Rad. 1981. "Cemented sands under static loading." *J. Geotech. Geoenviron. Eng.* 107 (6): 799–817. https://doi.org/10.1061/AJGEB6.0001152.

Cuthbert, M. O., L. A. McMillan, S. Handley-Sidhu, M. S. Riley, D. J. Tobler, and V. R. Phoenix. 2013. "A field and modeling study of fractured rock permeability reduction using microbially induced calcite precipitation." *Environ. Sci. Technol.* 47 (23): 13637–13643. https://doi.org/10.1021/es402601g.

Darby, K. M., G. L. Hernandez, J. T. DeJong, R. W. Boulanger, M. G. Gomez, and D. W. Wilson. 2019. "Centrifuge model testing of liquefaction mitigation via microbially induced calcite precipitation." *J. Geotech. Geoenviron. Eng.* 145 (10): 04019084. https://doi.org/10.1061/(ASCE)GT.1943-5606.0002122.

DeJong, J. T., M. B. Fritzges, and K. Nüsslein. 2006. "Microbially induced cementation to control sand response to undrained shear." *J. Geotech. Geoenviron. Eng.* 132 (11): 1381–1392. https://doi.org/10.1061/(ASCE)1090-0241(2006)132:11(1381).

DeJong, J. T., B. M. Mortensen, B. C. Martinez, and D. C. Nelson. 2010. "Bio-mediated soil improvement." *Ecol. Eng.* 36 (2): 197–210. https://doi.org/10.1016/j.ecoleng.2008.12.029.

DeJong, J. T., K. Soga, E. Kavazanjian, S. Burns, L. van Paassen, A. Al Qabany, and C. Y. Chen. 2013. "Biogeochemical processes and geotechnical applications: Progress, opportunities and challenges." In *Proc., 17th Géotechnique Symp. in Print*, 143–157. London: Institute of Civil Engineers Publishing.

De Muynck, W., D. Debrouwer, N. De Belie, and W. Verstraete. 2008. "Bacterial carbonate precipitation improves the durability of cementitious materials." *Cem. Concr. Res.* 38 (7): 1005–1014. https://doi.org/10.1016/j.cemconres.2008.03.005.

El Ghoraiby, M., H. Park, and M. T. Manzari. 2020. "Physical and mechanical properties of Ottawa F65 sand." In *Model tests and numerical simulations of liquefaction and lateral spreading*, 45–67. Cham, Switzerland: Springer.

Feng, K., and B. M. Montoya. 2016. "Influence of confinement and cementation level on the behavior of microbial-induced calcite precipitated sands under monotonic drained loading." *J. Geotech. Geoenviron. Eng.* 142 (1): 04015057. https://doi.org/10.1061/(ASCE)GT.1943-5606.0001379.

Ferris, F. G., V. Phoenix, Y. Fujita, and R. W. Smith. 2004. "Kinetics of calcite precipitation induced by ureolytic bacteria at 10 to 20°C in artificial groundwater." *Geochim. Cosmochim. Acta* 68 (8): 1701–1710. https://doi.org/10.1016/S0016-7037(03)00503-9.

Ferris, F. G., L. G. Stehmeier, A. Kantzas, and F. M. Mourits. 1996. "Bacteriogenic mineral plugging." *J. Can. Pet. Technol.* 35 (8): 56–61.

Frydman, S., T. Hendron, and H. Horn. 1980. "Liquefaction study of cemented sand." *J. Geotech. Eng.* 106 (3): 275–297. https://doi.org/10.1061/AJGEB6.0000933.

Fujita, Y., G. D. Redden, J. S. Ingram, M. M. Cortez, and R. W. Smith. 2004. "Strontium incorporation into calcite generated by bacterial ureolysis." *Geochim. Cosmochim. Acta* 68 (15): 3261–3270. https://doi.org/10.1016/j.gca.2003.12.018.

Gao, Y., L. Hang, J. He, and J. Chu. 2019. "Mechanical behaviour of biocemented sands at various treatment levels and relative densities." *Acta Geotech.* 14 (3): 697–707. https://doi.org/10.1007/s11440-018-0729-3.

Ghasemi, P., and B. M. Montoya. 2020. "Field application of the microbially induced calcium carbonate precipitation on a coastal sandy slope." In *Proc., Geo-Congress 2020: Biogeotechnics*, 141–149. Reston, VA: ASCE.

Gomez, M. G., C. M. Anderson, J. T. DeJong, D. C. Nelson, C. M. R. Graddy, and T. R. Ginn. 2017. "Large-scale comparison of bioaugmentation and biostimulation approaches for biocementation of sands." *J. Geotech. Geoenviron. Eng.* 143 (5): 04016124. https://doi.org/10.1061/(ASCE)GT.1943-5606.0001640.

Gomez, M. G., and J. T. DeJong. 2017. "Engineering properties of biocementation improved sandy soils." In *Proc., Grouting*, 22–33. Reston, VA: ASCE.

Gomez, M. G., J. T. DeJong, and C. M. Anderson. 2018a. "Effect of biocementation on geophysical and cone penetration measurements in sands." *Can. Geotech. J.* 55 (11): 1632–1646. https://doi.org/10.1139/cgj-2017-0253.

Gomez, M. G., C. M. Graddy, J. T. DeJong, and D. C. Nelson. 2019. "Biogeochemical changes during bio-cementation mediated by stimulated and augmented ureolytic microorganisms." *Sci. Rep.* 9 (1): 1–15. https://doi.org/10.1038/s41598-019-47973-0.

Gomez, M. G., C. M. Graddy, J. T. DeJong, D. C. Nelson, and M. Tsesarsky. 2018b. "Stimulation of native microorganisms for biocementation in samples recovered from field-scale treatment depths." *J. Geotech. Geoenviron. Eng.* 144 (1): 04017098. https://doi.org/10.1061/(ASCE)GT.1943-5606.0001804.

Gomez, M. G., B. C. Martinez, J. T. DeJong, C. E. Hunt, L. A. deVlaming, D. W. Major, and S. M. Dworatzek. 2015. "Field-scale bio-cementation tests to improve sands." *Proc. Inst. Civ. Eng. Ground Improv.* 168 (3): 206–216. https://doi.org/10.1680/grim.13.00052.

He, J., X. Chen, Q. Zhang, and V. Achal. 2019. "More effective immobilization of divalent lead than hexavalent chromium through carbonate mineralization by Staphylococcus epidermidis HJ2." *Int. Biodeterior. Biodegrad.* 140 (May): 67–71. https://doi.org/10.1016/j.ibiod.2019.03.012.

Hernandez, G. L. 2018. "Centrifuge model testing of liquefaction mitigation via microbially induced calcite precipitation." Master's thesis, Dept. of Civil and Environmental Engineering, Univ. of California.

Idriss, I. M., and R. W. Boulanger. 2008. *Soil liquefaction during earthquake*. Monograph MNO-12. Oakland, CA: Earthquake Engineering Research Institute.

Ishihara, K. 1993. "Liquefaction and flow failure during earthquakes." *Géotechnique* 43 (3): 351–451. https://doi.org/10.1680/geot.1993.43.3.351.

Ismail, M. A., H. A. Joer, W. H. Sim, and M. F. Randolph. 2002. "Effect of cement type on shear behavior of cemented calcareous soil." *J. Geotech. Geoenviron. Eng.* 128 (6): 520–529. https://doi.org/10.1061/(ASCE)1090-0241(2002)128:6(520).

Jiang, N. J., R. Liu, Y. J. Du, and Y. Z. Bi. 2019. "Microbial induced carbonate precipitation for immobilizing Pb contaminants: Toxic effects on bacterial activity and immobilization efficiency." *Sci. Total Environ.* 672 (Jul): 722–731. https://doi.org/10.1016/j.scitotenv.2019.03.294.

Karol, R. H. 2003. *Chemical grouting and soil stabilization, revised and expanded*. Boca Raton, FL: CRC Press.

Kendall, A., A. J. Raymond, J. Tipton, and J. T. DeJong. 2018. "Review of life-cycle-based environmental assessments of geotechnical systems." *Proc. Inst. Civ. Eng. Eng. Sustainability* 171 (2): 57–67. https://doi.org/10.1680/jensu.16.00073.

Lee, M., M. G. Gomez, M. El Kortbawi, and K. Ziotopoulou. 2020. "Examining the liquefaction resistance of lightly cemented sands using microbially induced calcite precipitation (MICP)." In *Proc., Geo-Congress 2020: Biogeotechnics*, 53–64. Reston, VA: ASCE.

Li, L., K. Wen, C. Bu, and F. Amini. 2020. "Enhancement of bio-sandy brick through discrete randomly distributed fiber." In *Proc., Geo-Congress 2020: Biogeotechnics*, 39–45. Reston, VA: ASCE.

Li, M., L. Li, U. Ogbonnaya, K. Wen, A. Tian, and F. Amini. 2016. "Influence of fiber addition on mechanical properties of MICP-treated sand." *J. Mater. Civ. Eng.* 28 (4): 04015166. https://doi.org/10.1061/(ASCE)MT.1943-5533.0001442.

Lin, H., M. T. Suleiman, H. M. Jabbour, D. G. Brown, and E. Kavazanjian Jr. 2016. "Enhancing the axial compression response of pervious concrete ground improvement piles using biogrouting." *J. Geotech. Geoenviron. Eng.* 142 (10): 04016045. https://doi.org/10.1061/(ASCE)GT.1943-5606.0001515.

Lings, M. L., and P. D. Greening. 2001. "A novel bender/extender element for soil testing." *Géotechnique* 51 (8): 713–717. https://doi.org/10.1680/geot.2001.51.8.713.

Martinez, B. C., and J. T. DeJong. 2009. "Bio-mediated soil improvement: Load transfer mechanisms at the micro- and macro-scales." In *Proc., 2009 US-China Workshop on Ground Improvement Technologies*. Reston, VA: ASCE.

Minto, J. M., E. MacLachlan, G. El Mountassir, and R. J. Lunn. 2016. "Rock fracture grouting with microbially induced carbonate precipitation." *Water Resour. Res.* 52 (11): 8827–8844. https://doi.org/10.1002/2016WR018884.

Mitchell, J. K. 2008. "Aging of sand—A continuing enigma?" In *Proc., 6th Int. Conf. on Case Histories in Geotechnical Engineering*, 1–21. Rollo, MO: Missouri Univ. of Science and Technology.

Mobley, H. L., M. D. Island, and R. P. Hausinger. 1995. "Molecular biology of microbial ureases." *Microbiol. Rev.* 59 (3): 451–480. https://doi.org/10.1128/mr.59.3.451-480.1995.

Montoya, B. M., and J. T. DeJong. 2015. "Stress-strain behavior of sands cemented by microbially induced calcite precipitation." *J. Geotech. Geoenviron. Eng.* 141 (6): 04015019. https://doi.org/10.1061/(ASCE)GT.1943-5606.0001302.

Montoya, B. M., J. T. DeJong, and R. W. Boulanger. 2013. "Dynamic response of liquefiable sand improved by microbial-induced calcite precipitation." *Géotechnique* 63 (4): 302–312. https://doi.org/10.1680/geot.SIP13.P.019.

Montoya, B. M., J. Do, and M. M. Gabr. 2018. "Erodibility of microbial induced carbonate precipitation-stabilized sand under submerged impinging jet." In *Proc., IFCEE 2018*, 19–28. Reston, VA: ASCE.

Morales, B., F. Humire, and K. Ziotopoulou. 2020. *Cyclic direct simple shear testing of Ottawa F-50 and F-65 sands*. DesignSafe-CI. Alexandria, VA: National Science Foundation.

Nafisi, A., B. M. Montoya, and T. M. Evans. 2020. "Shear strength envelopes of biocemented sands with varying particle size and cementation level." *J. Geotech. Geoenviron. Eng.* 146 (3): 04020002. https://doi.org/10.1061/(ASCE)GT.1943-5606.0002201.

Phillips, A. J., et al. 2016. "Fracture sealing with microbially-induced calcium carbonate precipitation: A field study." *Environ. Sci. Technol.* 50 (7): 4111–4117. https://doi.org/10.1021/acs.est.5b05559.

Puppala, A. J., Y. B. Acar, and K. Senneset. 1993. "Cone penetration in cemented sands: Bearing capacity interpretation." *J. Geotech. Eng.* 119 (12): 1990–2002. https://doi.org/10.1061/(ASCE)0733-9410(1993)119:12(1990).

Rad, N. S., and G. W. Clough. 1982. *The influence of cementation on the static and dynamic behavior of sands*. Rep. No. 59. Stanford, CA: John A. Blume Earthquake Engineering Center, Stanford Univ.

Rad, N. S., and M. T. Tumay. 1986. "Effect of cementation on the cone penetration resistance of sand: A model study." *Geotech. Test. J.* 9 (3): 117–125. https://doi.org/10.1520/GTJ10617J.

Ramachandran, S. K., V. Ramakrishnan, and S. S. Bang. 2001. "Remediation of concrete using micro-organisms." *ACI Mater. J.* 98 (1): 3–9.

Ramakrishnan, V., S. S. Bang, and K. S. Deo. 1998. "A novel technique for repairing cracks in high performance concrete using bacteria." In *Proc., Int. Conf. on HPHSC*, 597–618. Reston, VA: ASCE.

Ramakrishnan, V., K. P. Ramesh, and S. S. Bang. 2001. "Bacterial concrete." In *Proc., SPIE 4234*, 168–176. Bellingham, WA: SPEI.

Riveros, G. A., and A. Sadrekarimi. 2020. "Liquefaction resistance of Fraser River sand improved by a microbially-induced cementation." *Soil Dyn. Earthquake Eng.* 131 (Apr): 106034. https://doi.org/10.1016/j.soildyn.2020.106034.

San Pablo, A. C. M., et al. 2020. "Meter-scale bio-cementation experiments to advance process control and reduce impacts: Examining spatial control, ammonium by-product removal, and chemical reductions." *J. Geotech. Geoenviron. Eng.* 146 (11): 04020125. https://doi.org/10.1061/(ASCE)GT.1943-5606.0002377.

Saxena, S., K. Reddy, and A. Avramidis. 1988. "Liquefaction resistance of artificially cemented sand." *J. Geotech. Eng.* 114 (12): 1395–1413. https://doi.org/10.1061/(ASCE)0733-9410(1988)114:12(1395).

Saxena, S. K., and R. M. Lastrico. 1978. "Static properties of lightly cemented sand." *J. Geotech. Geoenviron. Eng.* 104 (12): 1449–1464. https://doi.org/10.1061/AJGEB6.0000728.

Seagren, E. A., and A. H. Aydilek. 2010. "Biomediated geomechanical processes." In *Environmental microbiology.* 2nd ed., 319–348. Hoboken, NJ: Wiley.

Simatupang, M., M. Okamura, K. Hayashi, and H. Yasuhara. 2018. "Small-strain shear modulus and liquefaction resistance of sand with carbonate precipitation." *Soil Dyn. Earthquake Eng.* 115 (Dec): 710–718. https://doi.org/10.1016/j.soildyn.2018.09.027.

Stocks-Fischer, S., J. K. Galinat, and S. S. Bang. 1999. "Microbiological precipitation of $CaCO_3$." *Soil Biol. Biochem.* 31 (11): 1563–1571. https://doi.org/10.1016/S0038-0717(99)00082-6.

Tao, J., J. Li, X. Wang, and R. Bao. 2018. "Nature-inspired bridge scour countermeasures: Streamlining and biocementation." *J. Test. Eval.* 46 (4): 1376–1390. https://doi.org/10.1520/JTE20170517.

Ueda, K., R. Vargas, and K. Uemura. 2018. *LEAP-Asia-2018: Stress-strain response of Ottawa sand in cyclic torsional shear tests*. DesignSafe-CI. Alexandria, VA: National Science Foundation.

van Paassen, L. A., R. Ghose, T. J. M. van der Linden, W. R. L. van der Star, and M. C. M. van Loosdrecht. 2010. "Quantifying biomediated ground improvement by ureolysis: Large-scale biogrout experiment." *J. Geotech. Geoenviron. Eng.* 136 (12): 1721–1728. https://doi.org/10.1061/(ASCE)GT.1943-5606.0000382.

Wu, J., A. M. Kammerer, M. F. Riemer, R. B. Seed, and J. M. Pestana. 2004. "Laboratory study of liquefaction triggering criteria." In *Proc., 13th World Conf. on Earthquake Engineering*. Tokyo: International Association for Earthquake Engineering.

Xiao, P., H. Liu, A. W. Stuedlein, T. M. Evans, and Y. Xiao. 2019a. "Effect of relative density and biocementation on cyclic response of calcareous sand." *Can. Geotech. J.* 56 (12): 1849–1862. https://doi.org/10.1139/cgj-2018-0573.

Xiao, P., H. Liu, Y. Xiao, A. W. Stuedlein, and T. M. Evans. 2018. "Liquefaction resistance of bio-cemented calcareous sand." *Soil Dyn. Earthquake Eng.* 107 (Apr): 9–19. https://doi.org/10.1016/j.soildyn.2018.01.008.

Xiao, Y., H. Chen, A. W. Stuedlein, T. M. Evans, J. Chu, L. Cheng, N. Jiang, H. Lin, H. Liu, and H. M. Aboel-Naga. 2020. "Restraint of particle breakage by biotreatment method." *J. Geotech. Geoenviron. Eng.* 146 (11): 04020123. https://doi.org/10.1061/(ASCE)GT.1943-5606.0002384.

Xiao, Y., X. He, T. M. Evans, A. W. Stuedlein, and H. Liu. 2019b. "Unconfined compressive and splitting tensile strength of basalt fiber–reinforced biocemented sand." *J. Geotech. Geoenviron. Eng.* 145 (9): 04019048. https://doi.org/10.1061/(ASCE)GT.1943-5606.0002108.

Zamani, A., and B. M. Montoya. 2019. "Undrained cyclic response of silty sands improved by microbial induced calcium carbonate precipitation." *Soil Dyn. Earthquake Eng.* 120 (May): 436–448. https://doi.org/10.1016/j.soildyn.2019.01.010.

Ziotopoulou, K., J. Montgomery, A. M. Parra Bastidas, and B. Morales. 2018. "Cyclic response of Ottawa F-65 sand: Laboratory and numerical investigation." In *Proc., Geotechnical Earthquake Engineering and Soil Dynamics V (GEESDV 2018)*. Reston, VA: ASCE.